

Atmospheric forcing of the Oregon coastal ocean during the 2001 upwelling season

J. M. Bane,¹ M. D. Levine,² R. M. Samelson,² S. M. Haines,¹ M. F. Meaux,^{1,3}
N. Perlin,² P. M. Kosro,² and T. Boyd²

Received 9 August 2004; revised 5 August 2005; accepted 9 September 2005; published 27 October 2005.

[1] Meteorological conditions during an intensive oceanographic observational program in May through August 2001 along the central Oregon coast are described and related to larger-scale and longer-term conditions. Southward wind stresses of $0.05\text{--}0.1\text{ N m}^{-2}$ occurred roughly 75% of the time, with a sustained period of dominantly southward stress from mid-June through July. Wind variations were correlated with variations in the large-scale Aleutian Low and North Pacific High pressure centers; correlations with the continental Thermal Low were small. Intraseasonal oscillations in alongshore wind stress (periods near 20 days) correlated with the north-south position of the jet stream. These stress oscillations drove 20 day oscillations in upper ocean temperature, with a lag of roughly 5 days for maximum correlation and amplitudes near 4°C . The sum of sensible and latent air-sea heat fluxes was generally into the atmosphere through June, then weakly into the ocean thereafter, with fluctuations on synoptic timescales. Semidiurnal fluctuations in surface air temperature were observed at two northern moorings, apparently forced indirectly by nonlinear internal ocean tides. The diurnal cycle of wind stress was similar for both southward and northward wind conditions, with the diurnal alongshore fluctuation southward in the evening and northward in the morning. During southward winds the marine atmospheric boundary layer (MABL) was typically defined clearly by a strong temperature inversion, and a shallow stable internal boundary layer often formed within the MABL over cool upwelled waters, with surface air temperature roughly 1°C lower inshore than offshore. During northward winds, essentially no low-level temperature stratification was observed.

Citation: Bane, J. M., M. D. Levine, R. M. Samelson, S. M. Haines, M. F. Meaux, N. Perlin, P. M. Kosro, and T. Boyd (2005), Atmospheric forcing of the Oregon coastal ocean during the 2001 upwelling season, *J. Geophys. Res.*, *110*, C10S02, doi:10.1029/2004JC002653.

1. Introduction

[2] The predominantly southward late spring and summer winds along the Oregon coast drive an active and biologically productive upwelling system. During May–August 2001, observations were made of the central Oregon coastal ocean and lower atmosphere as part of the Coastal Ocean Advances in Shelf Transport (COAST) research program, sponsored by the National Science Foundation's Coastal Ocean Processes initiative [Smith and Brink, 1994; *Coastal Ocean Processes*, 1998]. The goal of COAST is to study cross-margin transport processes associated with wind-driven coastal upwelling. Since continental shelf oceans in general, and the central

Oregon coastal ocean in particular, are known to be strongly wind driven, meteorological measurements were an integral part of the COAST 2001 field program.

[3] Our purposes here are to give a descriptive overview of the meteorological forcing of the central Oregon coastal ocean during the summer 2001 COAST field experiment, and to present a preliminary analysis of the COAST 2001 meteorological and near-surface ocean observations. New results in this paper include an analysis of the separate influences of large-scale atmospheric pressure centers on the coastal wind fluctuations in the COAST region, a description of semidiurnal fluctuations in surface air temperature that are apparently forced indirectly by nonlinear internal ocean tides, a quantitative assessment of the influence of oceanic upwelling on coastal surface air temperature, in situ observations of a stable internal boundary layer within the marine atmospheric boundary layer over the cold upwelled water along the central Oregon coast, and a description of intraseasonal wind fluctuations with periods near 20 days that correlate with fluctuations in the north-south position of the jet stream and which strongly affect the near-surface ocean temperature field at similar periods.

¹Department of Marine Sciences, University of North Carolina, Chapel Hill, North Carolina, USA.

²College of Oceanic and Atmospheric Sciences, Oregon State University, Corvallis, Oregon, USA.

³Now at Global Change Data Center, NASA/Goddard Space Flight Center, Greenbelt, Maryland, USA.

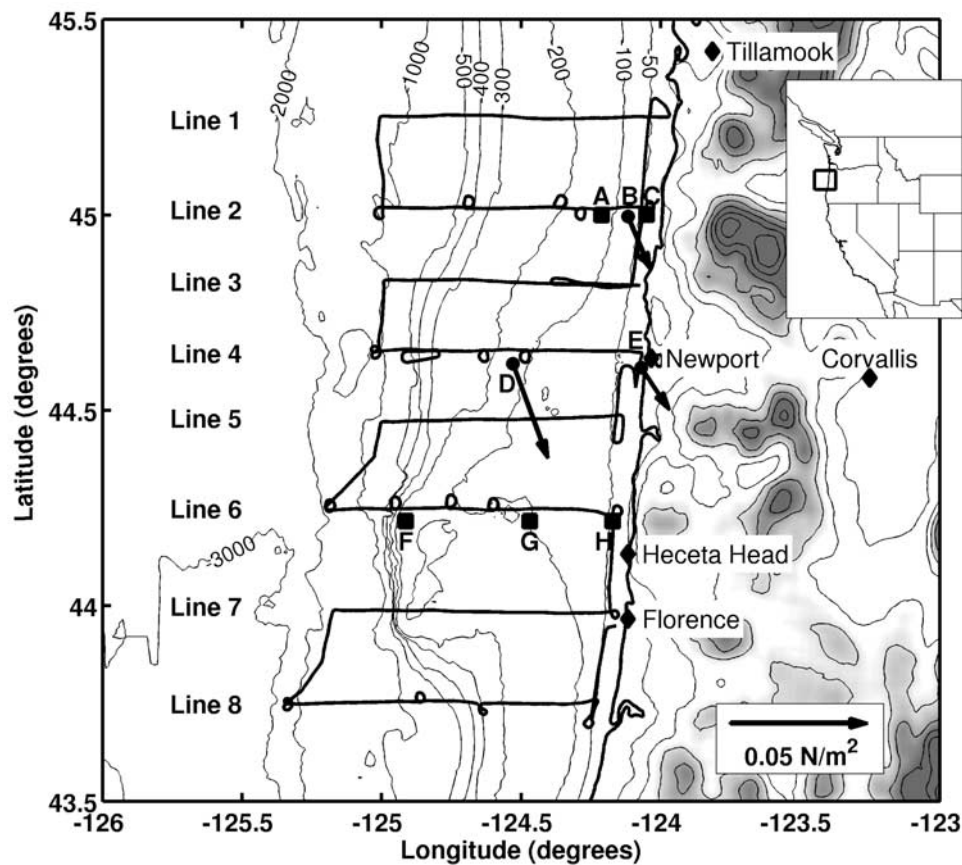


Figure 1. Map of the Coastal Ocean Advances in Shelf Transport (COAST) study area during summer 2001. A typical aircraft flight track is shown (the black line in a “radiator” pattern). Three oceanographic instrument moorings were located on line 2 (from west to east: NSB (A), NMS (colocated with the COAST MB (B)), and NIS (C)), and three were located on line 6 (from west to east: SSB (F), SMS (G), and SIS (H)). The three surface meteorological sites are shown as solid dots: the COAST MB on line 2 (B), the NDBC 46050 buoy on line 4 (D), and the NWPO3 C-MAN station at Newport (E). The mean wind stress for May through August at each met site is shown. Ocean bathymetric contours are in meters. The height contour interval over land is 500 m.

[4] Data sources are described next in section 2. In section 3 we place the COAST observations into the larger spatial and temporal context through the use of atmospheric pressure, wind and heat fluxes obtained from NCEP Eta forecast fields and the QuikSCAT satellite, and a 2 decade buoy record from the central Oregon coast. We show that variations in the large-scale atmospheric pressure systems over the eastern and northeastern North Pacific are the principal causes for the wind fluctuations that cause the variable upwelling and downwelling circulations in the Oregon coastal ocean, and that 2001 was a typical year in the COAST region in terms of wind stress. We then describe more fully the meteorological conditions during COAST 2001 in sections 4 and 5 using time series from surface buoys and observations from an instrumented aircraft. A summary is given in section 6.

2. Observational Data

2.1. Moored Surface Observations

[5] Figure 1 shows the seven sites where instrumented moorings were deployed for the 2001 COAST period [see also *Boyd et al.*, 2002]. Four moorings were arranged on an

east-west line across the shelf along 45°N and designated collectively as the North Array. Individually these were named, from west to east, North Shelf Break (NSB), COAST Meteorological Buoy (MB), North Mid Shelf (NMS), and North Inner Shelf (NIS). The distance between MB and NMS was less than 500 m, and they are treated as a single mooring for the present discussion. The South Array consisted of three moorings deployed across the shelf along 44°13'N, and these were individually named, from west to east, South Shelf Break (SSB), South Mid Shelf (SMS), and South Inner Shelf (SIS).

[6] Surface air temperature was measured at all locations except NMS and SSB using internally recording temperature loggers (Onset Computer Corp. 32K Stow-Away TidbiT TBI32-05+37), which were calibrated before and after deployment. Nominal accuracy and resolution are 0.2°C and 0.16°C, respectively. Each logger was mounted in a radiation shield supplied by the manufacturer, and each recorded temperature every 7.5 min. MB also had a more accurate temperature/relative humidity sensor (Vaisala Inc. HMP45C), which provided confidence in the accuracy of the Onset loggers. All air temperature sensors were mounted at a height of

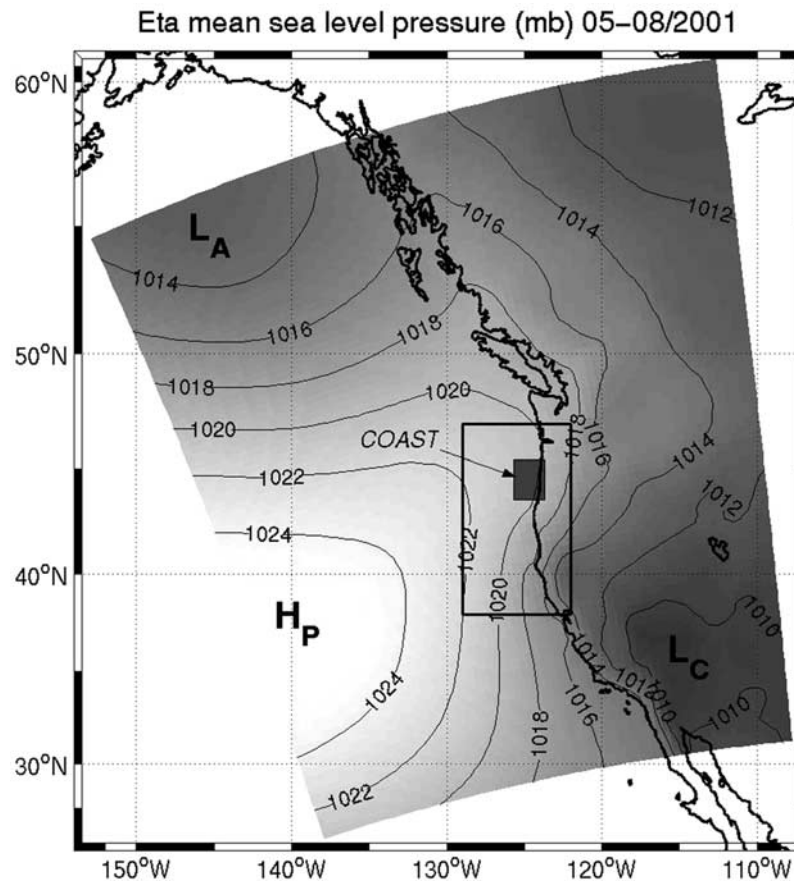


Figure 2a. Mean sea level pressure (mb) over the northeast Pacific during May through August 2001, from the NCEP Eta model. The three major atmospheric pressure systems that affected the COAST region during summer 2001 are the North Pacific High (H_P), the Thermal Low over the continent (L_C), and the Aleutian Low (L_A). The larger rectangular inset denotes the area shown in 2b, while the smaller inset indicates the location of the COAST summer 2001 field program.

3 m above the water, except at MB where they were at a height of 2.1 m.

[7] Near-surface water temperature was measured at all mooring sites but NMS with Sea-Bird Electronics sensors (SBE 39) at a depth of 2.4 m, except at MB where the sensor was located 1.5 m deep. At MB other meteorological variables were also measured, including incoming short-wave solar radiation (Li-Cor pyranometer LI200X) and wind velocity at 3 m height (R. M. Young 05103-5). Data were collected from two, long-term NOAA-NDBC sites as well (both shown in Figure 1). The NDBC 46050 buoy is located just south of line 4, about 35 km offshore of Newport on the 130 m isobath, and the NDBC NWPO3 C-MAN station is located on the beach at Newport. Sensor heights/depths, relative to sea level for NDBC 46050 (NWPO3) were as follows: air temperature, 4.0 m (15.5 m); anemometer, 5.0 m (18.5 m); ocean temperature, 0.6 m (N/A).

2.2. Aircraft Observations

[8] An instrumented, light twin-engine aircraft (Piper Seneca III) made repeated, in situ measurements of atmospheric wind, temperature, humidity and pressure, and it remotely sensed sea surface temperature (SST) and upper

ocean color. Additionally, AXBTs were deployed to measure subsurface ocean temperature down to 500 m. The aircraft provided rapid coverage of the study area, typically covering eight, 80–100 km cross-shore transects in about 6–7 hours (see Figure 1). Twenty-five flights were conducted between mid-May and the end of August 2001. Typical flight speeds ranged from about 50 m s^{-1} true airspeed during climbs, to 60 m s^{-1} in cruise and 70 m s^{-1} in descents, and altitudes ranged from 50 to 1000 m or more. Airspeed (measured with a Setra 239 differential pressure sensor) and heading (measured with a KVH C100 flux gate compass) accuracies of about 1 m s^{-1} and 2° , respectively, resulted in measured wind velocity accuracies of 2 m s^{-1} . Air temperature accuracy is about 0.3°C (Rosemount 102E4AL total temperature sensor), and SST accuracy is about 0.25°C (Heitronics KT-19.85 IR radiometer). Sensors, calibration procedures and data processing techniques are documented by Bane *et al.* [1995] (see http://www.marine.unc.edu/cool/coast/data_report; see also <http://www.marine.unc.edu/cool/COAST>).

2.3. Additional Data Sources

[9] Limited use is made in the following of data from three other sources: the NCEP reanalysis [Kalnay *et al.*,

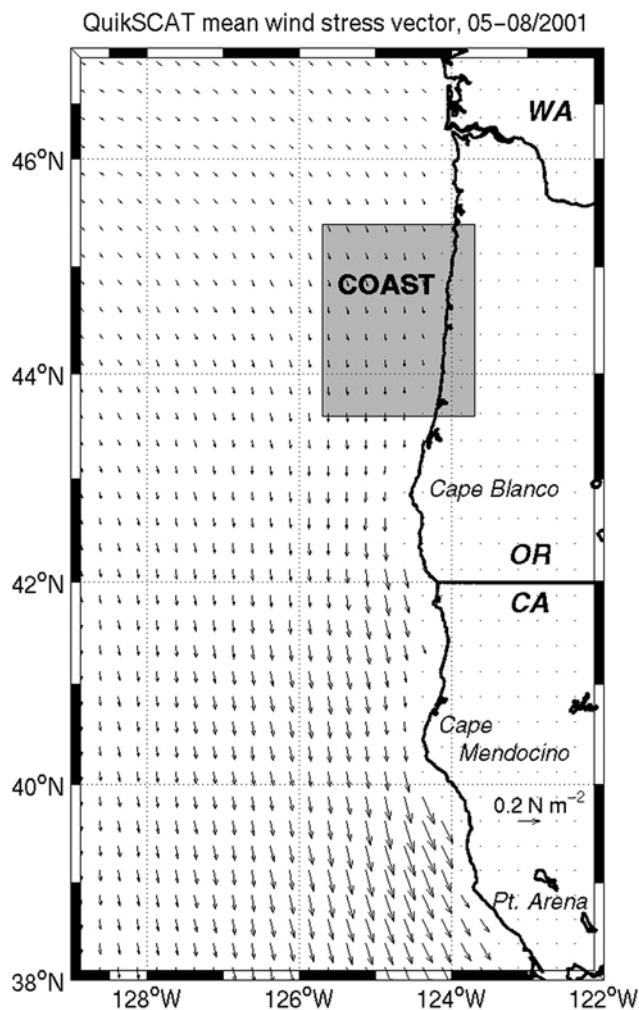


Figure 2b. Mean surface wind stress vectors over the ocean off Oregon and northern California during May through August 2001, from the QuikSCAT scatterometer. (Data were analyzed following the methods described by *Perlin et al.* [2004].)

1996], locally archived NCEP Eta model forecast fields [Black, 1994], and QuikSCAT satellite scatterometer data [Liu, 2002; Naderi et al., 1991]. NCEP Eta and QuikSCAT scatterometer wind stress fields have been compared for this region by *Perlin et al.* [2004]. The NCEP Eta surface heat flux fields described herein depend on the Eta model SST fields, which for summer 2001 were obtained from the RTG SST product [Thiébaux et al., 2003], a daily $0.5^\circ \times 0.5^\circ$ blend of satellite, buoy, and ship data plus climatology, which can be expected to capture the large-scale (>50 km) cooling associated with coastal upwelling, but not the details of individual events or mesoscale structure. The Eta model and QuikSCAT satellite fields were analyzed following the methods of *Perlin et al.* [2004].

3. Long-Term, Large-Scale Context

[10] Here we place the COAST observations into the longer-term and larger-scale atmospheric context. We begin by assessing how typical 2001 was for the COAST study

area. To do this, we constructed an 11 year ensemble of May–August surface wind stress statistics from NDBC 46050 using the years 1992 through 2004, but excluding 1996 and 1997 due to insufficient data. Stress was computed for each year using the procedure of *Large and Pond* [1981] and assuming neutral stability. Neutral stability was assumed due to data constraints from the NDBC buoy (humidity not available); however, we note that a comparison between two stress time series computed with data from MB (which had sensors sufficient to take stability into account) showed an rms difference of less than 10% between the two, one computed according to *Large and Pond* [1981] and assuming neutral stability and one computed with *Fairall et al.* [1996] using the observed stability. This difference is about the same as the uncertainties typically associated with bulk formula flux computations.

[11] It is interesting to note that the difference in along-shore stress calculated using the two methods was greater during northward winds than during southward winds. This is true for both the mean stress and the rms stress, and it is because the lower atmosphere was closer to neutral stability during southward winds. Southward (northward) winds are upwelling (downwelling) favorable, and the SST is generally cooler (warmer) then. The mean and rms alongshore stress values, in N m^{-2} , for the two cases are as follows (τ_{SC} is stability corrected, τ_{N} assumes neutral stability): For southward winds (78 daily values), $\tau_{\text{SC}}(\text{mean}) = -0.045$, $\tau_{\text{N}}(\text{mean}) = -0.045$, $\tau_{\text{SC}}(\text{rms}) = 0.033$, $\tau_{\text{N}}(\text{rms}) = 0.030$; and for northward winds (28 daily values), $\tau_{\text{SC}}(\text{mean}) = 0.052$, $\tau_{\text{N}}(\text{mean}) = 0.048$, $\tau_{\text{SC}}(\text{rms}) = 0.057$, $\tau_{\text{N}}(\text{rms}) = 0.050$. Additionally, the rms difference between the two methods was 0.004 for southward winds, and for northward winds it was 0.007.

[12] The 2001 mean northward wind stress was -0.035 N m^{-2} (i.e., a stress toward the south, calculated for all days and assuming neutral stability), which compares well with the long-term mean for the 11 year ensemble of -0.031 . The maximum (weakest southward stress) and minimum (strongest southward stress) mean northward stress for May–August for all 11 years were -0.019 (1993) and -0.040 (1992), respectively. The maximum, hourly averaged northward stress for any year was 0.560 (2001), and the minimum hourly averaged northward stress was -0.384 (1999). For the eastward stress component, the 2001 mean for May–August was 0.013 (i.e., an eastward stress), while the 11 year ensemble mean was 0.010 . 2001 had neither the minimum nor the maximum hourly averaged eastward stress for the entire, 11 year ensemble. Together these statistics indicate that 2001 was slightly on the strong side for both wind stress components, but it was not an extreme year, with the exception of having the strongest hourly averaged stress to the north. This was due to the transit of an extratropical cyclone past the COAST area during mid-May, and although the peak stress was high, it was short lived (see Figure 4 below).

[13] The mean surface pressure field over the eastern North Pacific and western North America during May–August 2001 comprised the North Pacific High, the Aleutian Low, and the Thermal Low over the continent to the southeast (H_P , L_A and L_C , respectively, in Figure 2a). The Aleutian Low region seen here is in large part the signature left in the mean pressure field by a sequence of synoptic-

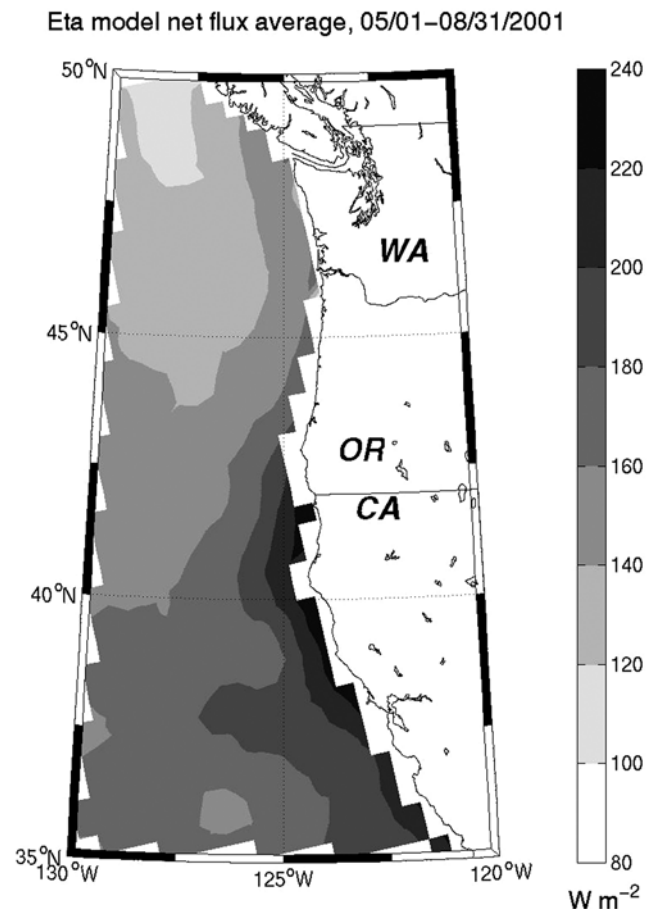


Figure 3a. Mean net heat flux into the ocean over the northeast Pacific during May through August 2001, from the NCEP Eta model.

scale, extratropical low-pressure systems (often referred to as Gulf of Alaska Lows) that progressed west-to-east through this region throughout the COAST period. The nearly geostrophic winds associated with the pressure gradient between the northeastern part of the North Pacific High and the northwestern part of the Thermal Low give a mean wind stress field that is southward and coastal-upwelling-favorable along the Oregon and the northern and central California coasts. Figure 2b shows the mean wind stress field has a large-scale maximum that extends from southern Oregon to central California, arising from the intensified geostrophic winds offshore of the Thermal Low, and smaller-scale orographic intensifications near Capes Blanco and Mendocino [e.g., *Winant et al.*, 1988; *Edwards et al.*, 2001; *Samelson et al.*, 2002; *Perlin et al.*, 2004]. The COAST area is positioned near the northern extent of the southward mean coastal winds, close to the transition between the North Pacific High and the Aleutian Low. In this location, the anticyclonic turning of the stress vectors around the northeastern corner of the high is apparent, a characteristic that can be seen in the mean buoy-measured winds as well (Figure 1).

[14] Mean net (Figure 3a) and sensible-plus-latent (Figure 3b) Eta model air-sea heat fluxes for the study period indicate that the upper ocean absorbed heat through-

out the entire area of interest, while mean southward advection of cold air over the area drove mean sensible-plus-latent heat fluxes from the ocean to the atmosphere. The magnitudes of these latter fluxes were typically only a small fraction of the total, which was dominated by insolation. In much of the coastal zone, oceanic upwelling induced by the southward wind stress reduced the ocean-to-atmosphere fluxes of sensible-plus-latent heat. This was the case for the COAST region, where the mean net Eta heat flux was between 160 and 180 W m^{-2} into the ocean, mostly from insolation. The averaged sensible-plus-latent heat flux was about 20 W m^{-2} out of the ocean.

4. Temporal Variations During Summer 2001

4.1. Wind Stress and Surface Heat Fluxes

[15] Surface winds off Oregon generally contain a substantial southward mean component during the upwelling season, and they reverse more frequently to northward than the winds along the northern and central California coast [*Halliwel and Allen*, 1987]. This greater variability is due primarily to the fact that the Oregon coastal zone is closer to the transition between the North Pacific High and the Aleutian Low (Figure 2a), and so is more often subjected to the influence of eastward traveling Gulf of Alaska Lows.

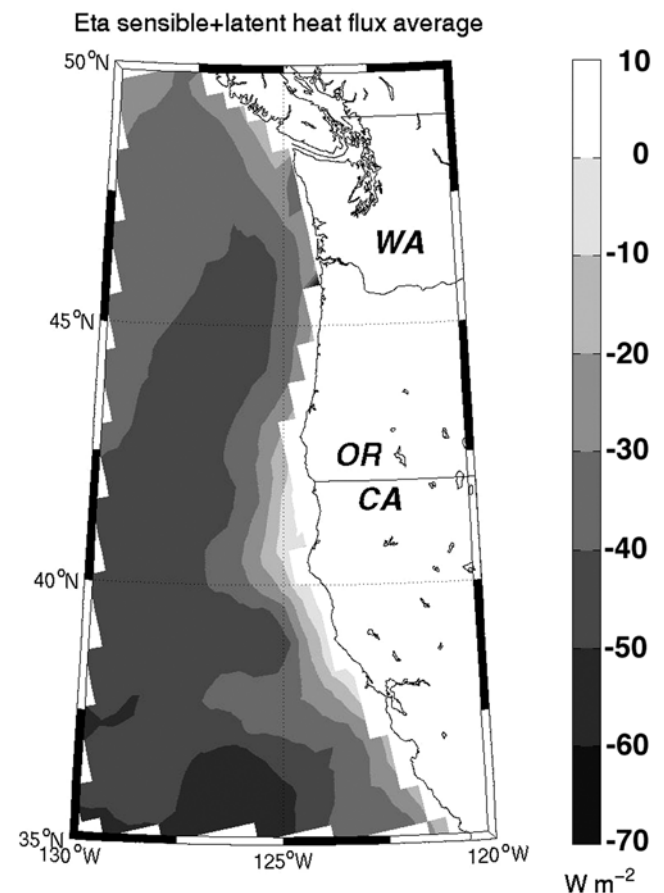


Figure 3b. Mean sensible-plus-latent heat flux from the atmosphere into the ocean during May through August 2001, from the NCEP Eta model. Negative values indicate that the atmosphere was receiving heat from the ocean.

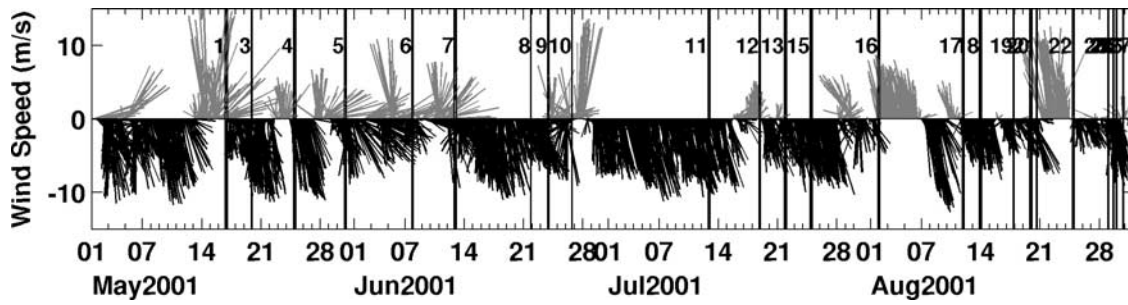


Figure 4. Time series of six-hourly wind velocity vectors at the NDBC 46050 buoy. True north is up. Southward, upwelling-favorable winds are depicted in black, and northward, downwelling-favorable winds are shown in shading. Winds were southward 75% of the time, while 15 northward wind episodes accounted for the other 25% of the record. Aircraft flight times are denoted by the vertical lines.

During May–August 2001, periods of persistent $5\text{--}7\text{ m s}^{-1}$ southward winds lasted from several days to 2 weeks and were interrupted by episodes of northward winds that typically lasted 1–3 days, although a longer period of northward winds occurred in early August (Figure 4). Time series of bulk air-sea fluxes and wind stress were computed from MB using measured wind velocity, surface air temperature (SAT), near-surface ocean temperature and relative humidity, following *Fairall et al.* [1996]. A wind stress time series was also computed from NDBC 46050 data following *Large and Pond* [1981] and assuming neutral stability. Figure 5a shows that the wind stress was nearly uninterrupted toward the south at $0.05\text{--}0.1\text{ N m}^{-2}$ from mid-June through the end of July, while stress fluctuations and reversals were more frequent during mid-May through

mid-June and during August. Figure 5b shows the time series of daily-averaged latent heat flux and sensible heat flux from the COAST meteorological study.

[16] Fluctuations in coastal wind and wind stress in the COAST region were closely related to fluctuations in the three, large-scale atmospheric pressure systems identified above, through their separate effects on the large-scale, cross-shore pressure gradients and alongshore geostrophic winds. This result follows from an analysis of empirical orthogonal functions (EOFs) computed separately for the surface pressure fields in regions associated with the North Pacific High, the Aleutian Low, and the Thermal Low (Figure 6). In each case, the leading EOF explains a large fraction of the variance in the corresponding region. Correlations of the amplitudes of these leading EOFs with the

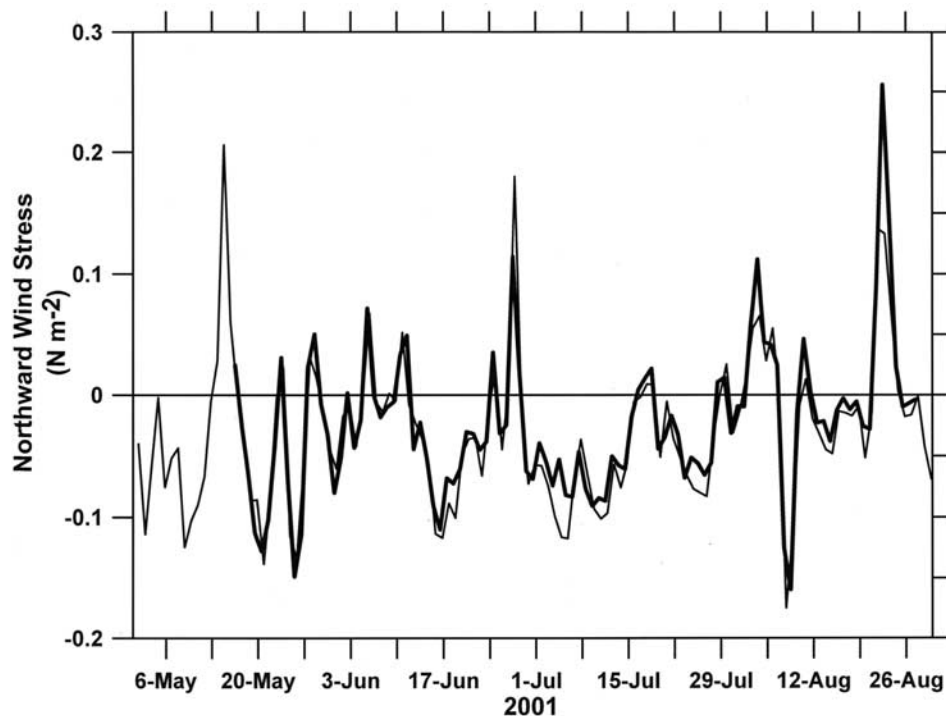


Figure 5a. Time series of daily averaged northward wind stress from the COAST MB (bold line) and from NDBC 46050 (thin line). Extended periods of southward, upwelling-favorable wind stress were interrupted by episodes of northward stress.

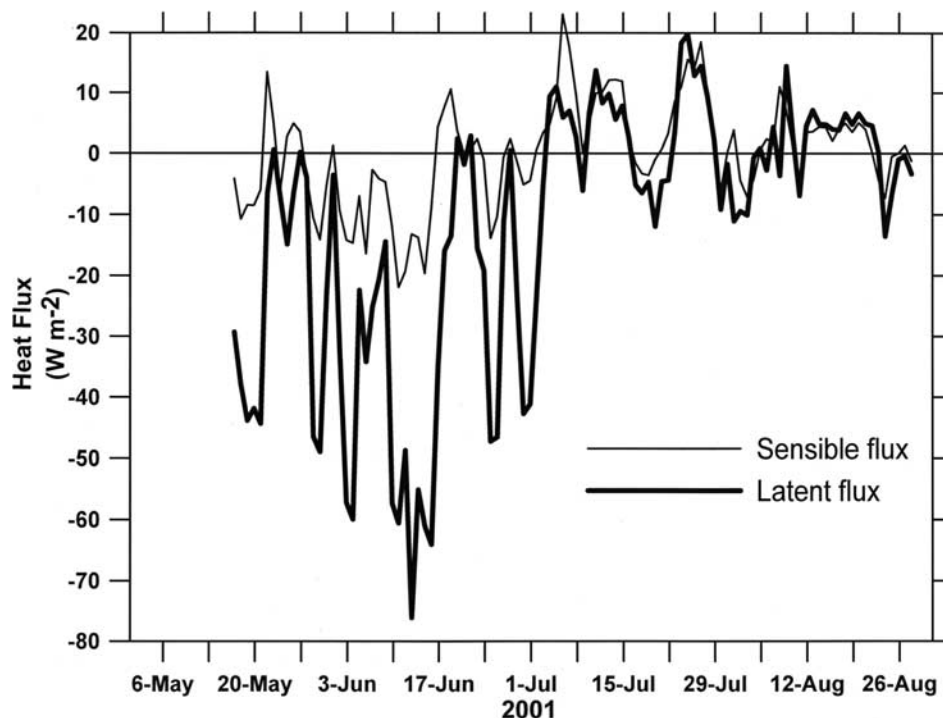


Figure 5b. Time series of daily averaged latent heat flux (bold) and sensible heat flux (thin) from the COAST meteorological buoy (MB). During the first half of COAST, these fluxes were almost exclusively from the ocean into the atmosphere (negative). The seasonal increase in air temperature coupled with the upwelling-induced cooling of the upper ocean caused a reversal in these fluxes during the second half of COAST, so they were mostly from the atmosphere to the ocean then.

time series of alongshore wind stress, where the alongshore direction is defined by the local major axis of wind stress variability, at NDBC buoys along the U.S. west coast reveal that the influences of the first two pressure centers vary strongly along the coast (Figure 7). Correlations are high with the Aleutian Low to the north of COAST and with the North Pacific High along Oregon and northern California, while the Thermal Low fluctuations are not strongly correlated with buoy records at any location shown. Although variability in the Thermal Low has been implicated in the development of summertime coastally trapped wind reversals [Nuss *et al.*, 1999], the present analysis suggests that it plays a relatively minor role among the large-scale processes that control variations in the upwelling winds along much of the U.S. west coast. Instead, it is the fluctuations in the North Pacific High and the Aleutian Low that dominate.

[17] An examination of NCEP reanalysis weather maps throughout the COAST study period helped identify many of the specific events that produced the observed wind fluctuations. This examination found that the 15 northward wind episodes during May–August (Figures 4 and 5a) can be attributed to the following: 11 Gulf of Alaska Lows transiting the region, 2 coastally trapped wind reversals, and 2 local disturbances, the nature of which could not be determined from the NCEP data. One of the low-pressure systems that we have included in the Gulf of Alaska Low category (the one which brought strong northward winds to COAST during 21–24 August) was actually a cyclone that

evolved from a tropical low-pressure system that had developed earlier in the western Pacific (M. W. Ott *et al.*, Summertime downwelling off the Oregon coast, submitted to *Journal of Geophysical Research*, 2005).

[18] Time series of latent and sensible heat fluxes from MB show a marked transition in early July (Figure 5b). The sum of these two fluxes was negative (cooling the ocean) during most of May and June, and then weakly positive (heating the ocean) during much of July and August. This shift in heat fluxes arose from a combination of a slow warming trend in the surface air temperature and repeated episodes of upwelling of cold water along the coast. The latter essentially eliminated the coastal ocean as a heat source by early July. The shorter timescale fluctuations in these fluxes were principally due to the changing synoptic conditions in the study region, caused mostly by Gulf of Alaska Lows impacting the area and altering the winds. The mean sensible heat flux for May through August at MB was near zero, while the mean latent heat flux was -12 W m^{-2} , consistent with the mean distribution shown in Figure 3b.

[19] The bulk formula computations used here indicate fluxes of latent heat into the ocean at times after 1 July (Figure 5b). These must arise from condensation at or near the sea surface under conditions that are often accompanied by fog. Similar estimates of downward latent heat flux have been derived previously from coastal observations [e.g., Beardsley *et al.*, 1998]; however, these results are sensitive to the measured values of the relative humidity and temper-

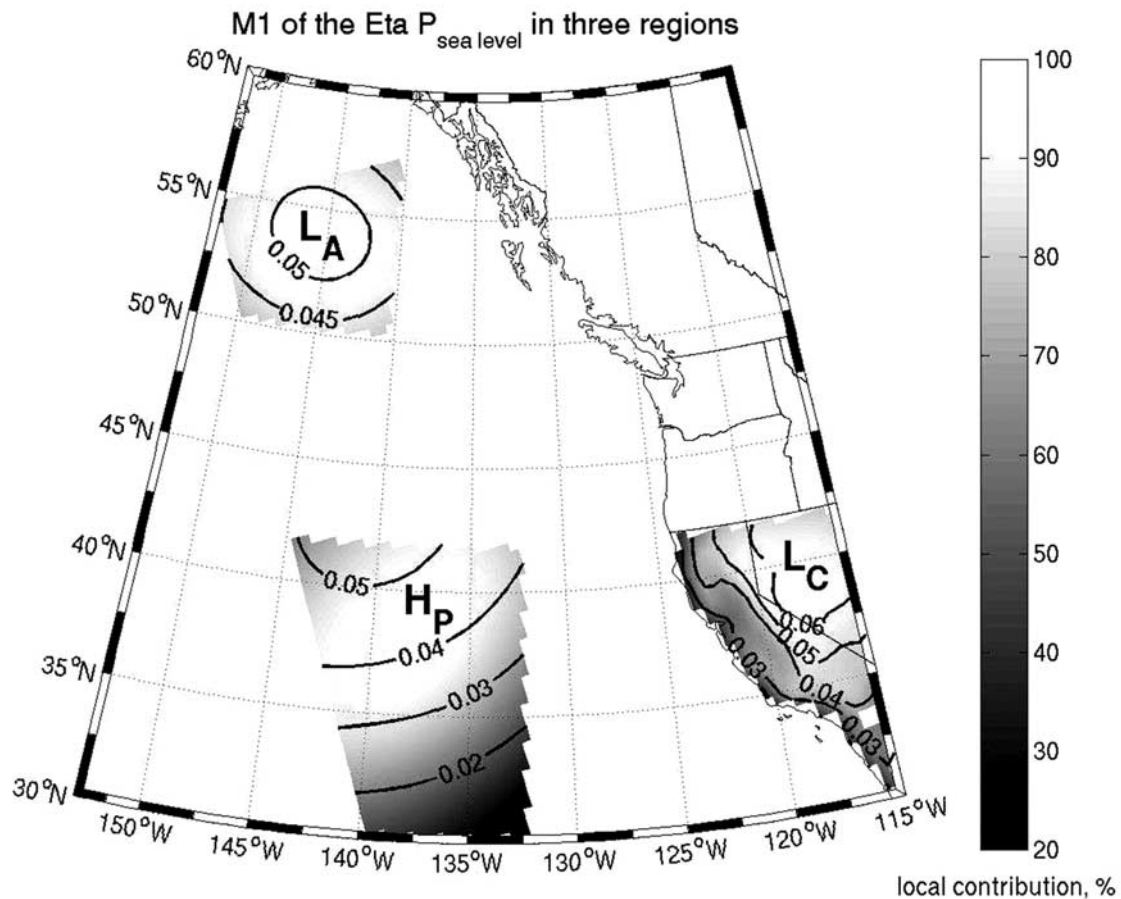


Figure 6. Leading empirical orthogonal functions (EOFs) of sea level pressure (labeled contours), with percent variance explained (shading), computed separately in the regions of the Aleutian Low (L_A), the North Pacific High (H_P), and continental Thermal Low (L_C).

ature, and bulk formula are not designed for foggy conditions. Therefore these results should be treated with caution.

4.2. Diurnal and Semidiurnal Fluctuations in Surface Air Temperature and Upper Ocean Temperature

[20] Spectra of SAT at the five mooring locations are generally similar. They are characterized by a large diurnal (0.042 cph) peak, with a power law decay toward higher frequencies (roughly ω^{-2}) and a less regular red spectrum toward lower frequencies (Figure 8). However, at NIS and NMS/MB, there are also significant peaks (at the 95% level) at the semidiurnal (0.083 cph) frequency. The diurnal fluctuations, seen throughout the study area, are presumably forced directly by solar heating. The existence of relatively strong semidiurnal fluctuations of SAT at NIS and NMS/MB, on the other hand, is surprising. We argue below that these oscillations appear to be forced by fluctuations in upper ocean temperature that are created by the passage of shoreward propagation of nonlinear internal wave packets generated by the semidiurnal ocean tide. Spectra of near-surface water temperature also show diurnal peaks at all of the moorings, and strong semidiurnal peaks at NIS and NMS/MB (Figure 9).

[21] Coherences between SAT and near-surface ocean temperature in the diurnal frequency band at the same location are significantly nonzero at all moorings. In the

semidiurnal frequency band, significantly nonzero coherences were observed at NIS, NMS/MB, and SIS (Figure 10). This coherence is consistent with the forcing of the SAT by the near-surface ocean temperature changes due to the internal tide. At lower frequencies the coherences are only marginally significant, except in the frequency band near 0.002 cph (20 day period) where coherences are high and significantly nonzero at all locations except SSB. This latter, intraseasonal signal is discussed further below in section 4.4.

[22] A particularly striking example showing the coherence of the semidiurnal fluctuations in SAT and near-surface ocean temperature occurred during days 200–204 at NIS (Figure 11). Upper ocean temperature often changed by 2°–4°C in a few minutes, apparently at the sharp leading edge of a nonlinear internal wave packet. The 1.7 hour time difference between these events at NMS and NIS yields an onshore propagation speed of roughly 0.6 m s⁻¹, slightly higher than that expected for a mode 1 internal wave. At times during this period and others, the near-surface ocean temperature was warmer than the SAT, producing an unstable region in the lower part of the atmospheric boundary layer that persisted for up to several hours.

[23] Comparable semidiurnal fluctuations were not found at other COAST mooring sites, indicating perhaps that the shallowness and sharpness of the oceanic thermocline at NIS and NMS/MB allowed the internal wave effects to be

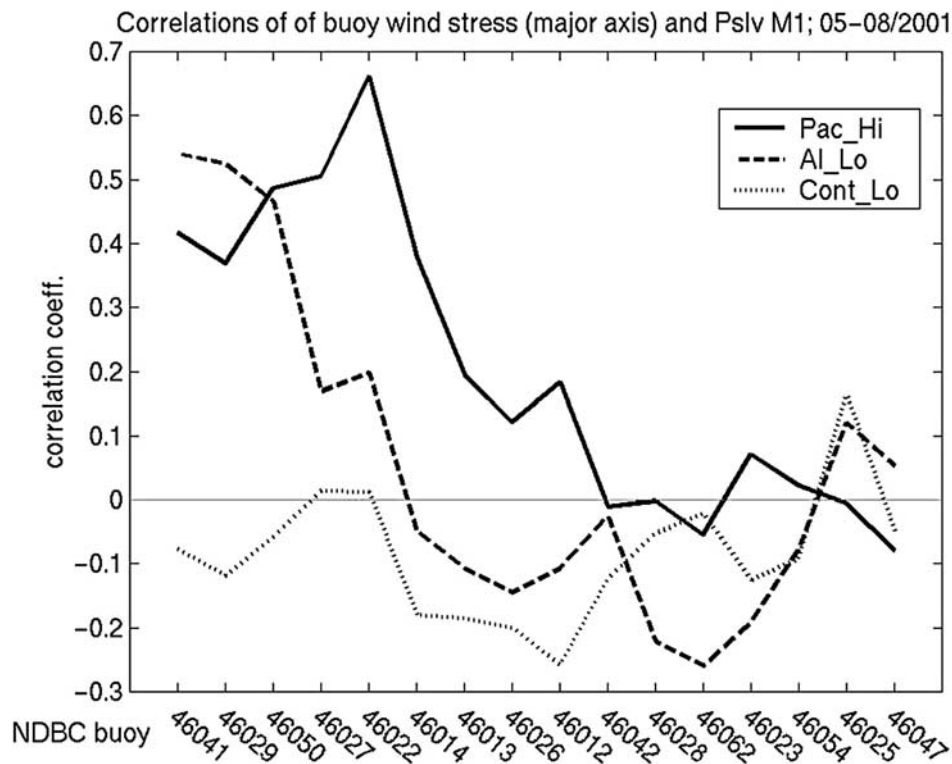


Figure 7. Correlations of the leading EOF amplitudes for the sea level pressure EOFs in Figure 6 with several NDBC buoy alongshore wind stress time series, where the alongshore direction is defined by the local major axis of wind stress variability. Stresses were computed using the *Large and Pond* [1981] bulk formula with neutral stability for the indicated buoys along the U.S. west coast. The buoys are ordered sequentially from north to south (left to right) along the horizontal axis. NDBC 46050 is located off the central Oregon coast (Figure 1), NDBC 46013 is located between Pt. Arena and San Francisco, NDBC 46042 is off Monterey Bay, and NDBC 46054 is in the Southern California Bight, near Pt. Conception.

seen so clearly at the surface. Since the semidiurnal tide is dominated by the M2 component (12.42 hours), the phasing between the solar day and tide changes over time. During 19–23 July (Figure 11), the peaks of the tide are nearly in phase with local noon and midnight. The warming of the ocean and air associated with the midnight peaks is clearly not due to solar radiation, indicating an oceanic source for the warming. The nonlinear semidiurnal internal tides, clearly evident in the subsurface thermistor records, are the most likely candidates.

4.3. Diurnal Cycle of the Wind

[24] Spectra of zonal (u) and meridional (v) wind at MB and NDBC 46050 have quite different levels below the diurnal frequency, with the v component variance about 9 times greater than that for the u component at MB (Figure 12). About 90% of the variance in the v component comes from below the diurnal frequency, and these fluctuations are discussed above in section 4.1 and below in section 4.4. There are only hints of semidiurnal peaks in these spectra, but the diurnal peak is quite distinct.

[25] The mean diurnal variations in wind stress components and sea level pressure at NDBC 46050 were computed by averaging these variables at each hour of the day for all days during May–August 2001 (Figure 13). Averaging in this fashion gives a curve which shows the mean diurnal

cycle plus the record-long mean for each variable (e.g., the mean southward stress is apparent in Figure 13). The maximum southward stress was reached during early evening (0300–0500 UTC, 2000–2200 PDT), and the minimum southward stress occurred during midmorning (1600–1900 UTC, 0900–1200 PDT). The diurnal eastward stresses were weaker, with an afternoon maximum occurring near 0000 UTC (1700 PDT) and a morning minimum near 1600 UTC (0900 PDT). The mean diurnal variation of wind stress during COAST agrees well, in both amplitude and phase, with that for June–August 1999 reported by *Samelson et al.* [2002], although the record-long mean value for each stress component was about 20% less for 1999 than for 2001.

[26] The increase in mean eastward wind stress begins a couple of hours before the southward wind stress increases during the day, consistent with a sea-breeze-like circulation. *Johnson and O'Brien* [1973] previously observed a sea breeze circulation at and east of Newport during southward winds in the 1972 CUE-I program. They followed the inshore penetration of near-surface air more than 60 km inland and observed a return flow above the temperature inversion between 1000–1500 m (see section 5 below for a description of the temperature inversion during southward winds). Figure 1 shows that NDBC 46050 is directly west of the valley in the coastal mountain range through which *Johnson and O'Brien* [1973] followed the diurnal flow of

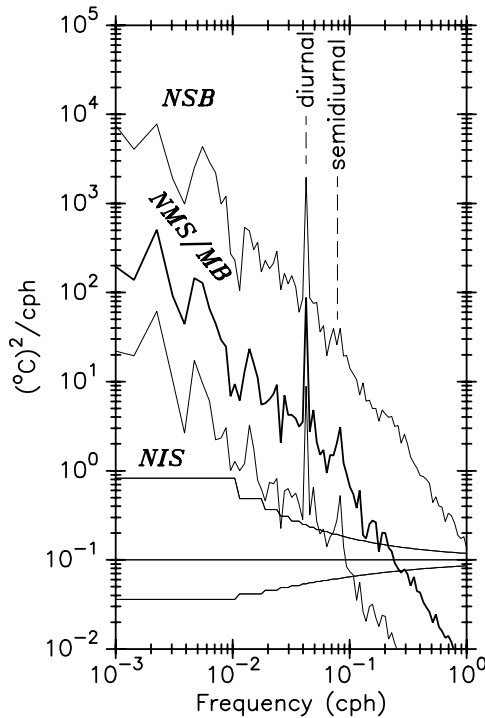


Figure 8. Spectra of moored surface air temperature (SAT) measured at NIS, NMS/MB, and NSB. Confidence limits (95%) are shown at the bottom.

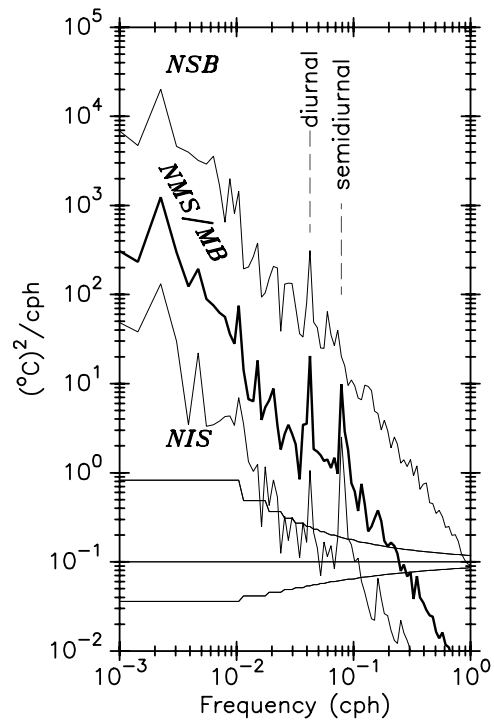


Figure 9. Spectra of near-surface ocean temperature measured at NIS, NMS/MB, and NSB. Confidence limits (95%) are shown at the bottom.

marine air, and so it is likely in a good position to capture the sea breeze oscillation. *Beardsley et al.* [1987] described a similar diurnal cycle in the winds off northern California during the CODE experiment, but preferred to call it the “daytime alongshore acceleration” as opposed to the sea breeze, due to the strong alongshore wind component. *Bielli et al.* [2002] used profiler observations and a regional atmospheric model to examine the diurnal circulation off central Oregon, and they noted that it was similar to that observed in the CODE region, but more complex in that it was fully three-dimensional, due to large alongshore gradients in the fluctuating alongshore wind that were apparently associated with diurnal heating over the high orography along the Oregon-California border. *Perlin et al.* [2004] provide support for this latter interpretation from an analysis of QuikSCAT observations.

[27] When the 2001 NDBC 46050 wind record is divided into periods of northward winds and periods of southward winds, it can be seen that the diurnal component has essentially the same phase and amplitude for each case (Figure 14). However, due to the different directions of the mean winds between the two cases, the total diurnal variation (mean plus diurnal component) has a different character during northward winds than during southward winds. During days with southward winds (about 75% of the time during COAST), the maximum alongshore wind stress typically occurred near sunset and the minimum alongshore stress occurred in the morning. During days with northward winds, it was the opposite: the maximum alongshore stress was during the morning and the minimum was near sunset. The maximum eastward wind stress in both cases (southward wind days and northward wind days)

occurred in the afternoon (near 0000 UTC, 1700 PDT), consistent with a sea-breeze-like circulation driven by daytime heating over land.

[28] The reason for this difference between northward and southward wind situations is as follows. Daytime heating

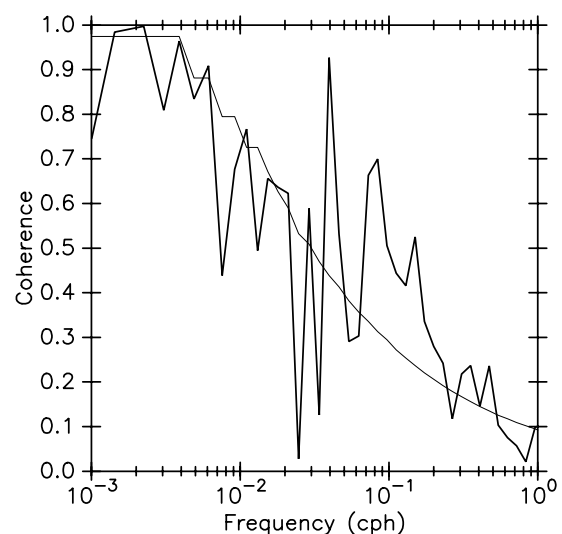


Figure 10. Spectral coherence between surface air temperature (SAT) and near-surface ocean temperature at NMS/MB. Values above the thin line are significantly nonzero at the 95% confidence limit using the standard null hypothesis test [*Koopmans*, 1974].

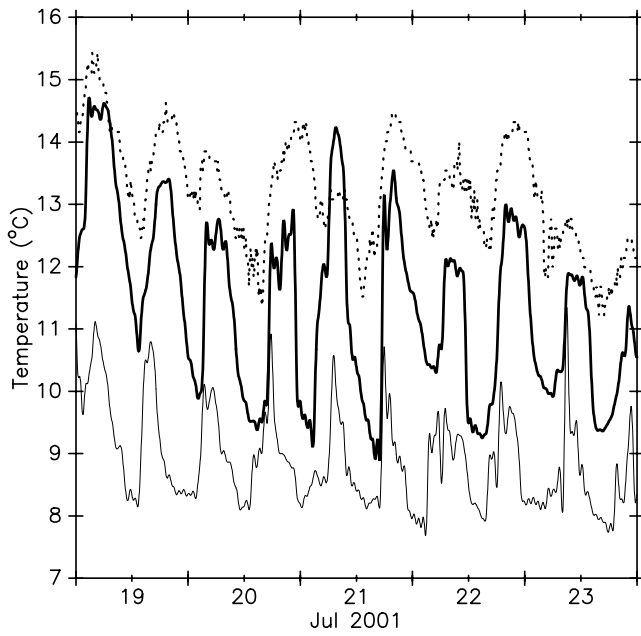


Figure 11. Surface air (SAT) and near-surface ocean temperatures at NIS during 5 days in July 2001. Curves are as follows: dashed, SAT; bold, ocean temperature at 2.4 m; thin, ocean temperature at 12 m.

and subsequent rising of the air over land drives the eastward afternoon, low-level flow during both southward and northward wind situations. This takes the dense, near-surface air from over the ocean toward inland areas, which

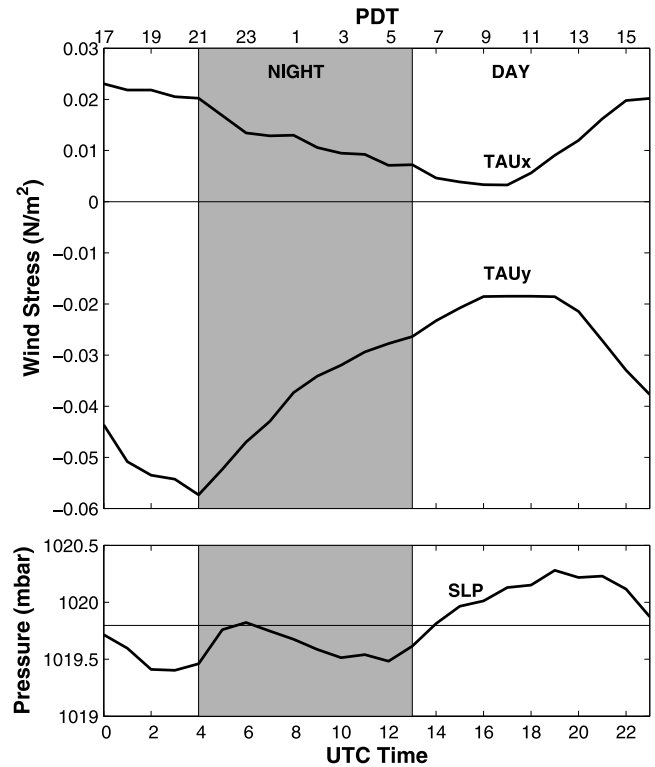


Figure 13. Mean diurnal variation of wind stress (τ_{Ux} and τ_{Uy}) and sea level pressure (SLP) at NDBC 46050. Shown are the mean variations for all days during May–August 2001. τ_{Ux} is positive toward true east, and τ_{Uy} is positive toward true north.

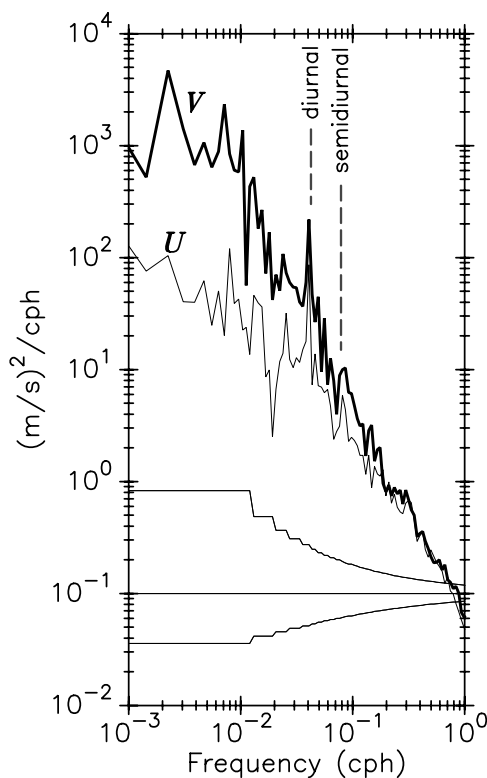


Figure 12. Spectra of zonal (u) and meridional (v) wind at MB. Confidence limits (95%) are shown at the bottom.

reduces the sea level pressure (SLP) over the coastal waters (see the SLP curve in Figure 13). During southward winds, the coastal SLP is lower than that offshore, so the further lowering of the SLP during this portion of the diurnal cycle enhances the magnitude of the east-west pressure gradient, resulting in a geostrophic increase in the southward wind speed. During northward winds, the coastal SLP is higher than that offshore, and so the diurnal lowering of the coastal SLP decreases the east-west pressure gradient magnitude, resulting in a geostrophic decrease in the northward wind speed. Note the correlation between low SLP and the strongest southward winds near sunset in Figure 13. This explanation is further supported by the results of *Bielli et al.* [2002], who showed that geostrophy is the dominant momentum balance in the cross-shore direction during southward winds in this region. The e -folding timescale for such a geostrophic adjustment is between f^{-1} and $(f Ro)^{-1}$, where f is the Coriolis parameter and Ro is the Rossby number [Reznik and Grimshaw, 2002]. For the latitude of COAST, this is a range of 3 hours to around a few days (assuming Ro between 0.05 and 0.1). Although the alongshore wind will not adjust completely to the changing horizontal pressure gradient force during that portion of the sea breeze cycle when the surface pressure is changing (dropping in the afternoon/evening, increasing in the morning), it will tend to adjust as much as the time period allows and in the direction observed (e.g., increas-

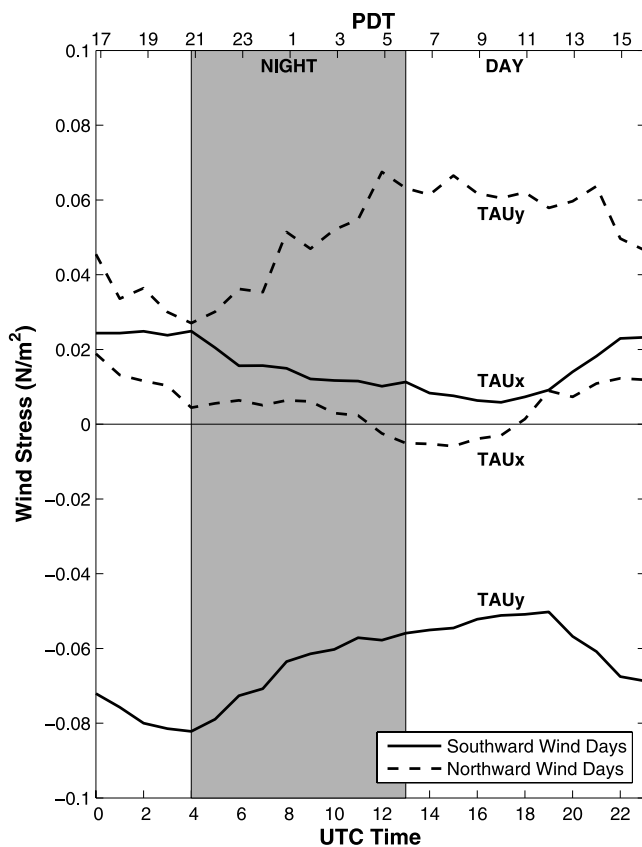


Figure 14. Mean diurnal variation of the wind stress at NDBC 46050 for days during May–August 2001 with only southward winds (solid curve), and the mean diurnal variation for days with only northward winds (dashed curves). TAU_x is positive toward true east, and TAU_y is positive toward true north.

ing southward wind strength during the afternoon on a day when southward winds prevail).

4.4. Intraseasonal Oscillations

[29] A sequence of upper ocean temperature oscillations with periods near 20 days and peak-to-peak amplitudes of about 4°C was observed throughout the COAST moored instrument array. Four to five such oscillations occurred at each of the six moorings and at NDBC 46050, and they occupied almost the entire field experiment time frame. These are intraseasonal oscillations (ISOs), and they can be seen in Figure 15 for SMS (see also Figure 18, below, which displays the ISO signatures at the three moorings in the North Array). They were the dominant temperature oscillation at each mooring location. Although upwelling episodes driven by southward winds bring cold water to the surface and thus change ocean surface temperature, the roughly 20 day timescale of these temperature oscillations is much longer than the average 7 day period it takes for the winds to undergo an “upwelling cycle,” a period of southward winds, ending with a reversal to northward winds, and then a change back to southward winds (5.3 days average southward wind episode and 1.8 days average northward wind episode during COAST). The 8 day low-

pass (8-DLP) filtered alongshore wind stress time series from NDBC 46050, however, does show a strong component with near-20-day periodicities (Figure 15, top and bottom). The correlation between the 8-DLP wind stress and the 8-DLP surface ocean temperature is maximum when the stress time series is lagged by roughly 5 days (Figure 15, next to bottom). It is interesting to note that the 20 day ISOs in the upper ocean temperature time series are the largest fluctuations in near-surface ocean temperature in terms of peak-to-peak amplitudes. In contrast, the unfiltered wind stress time series has shorter-period fluctuations that rival the 20 day stress ISOs in amplitude. The 8-DLP, 5-day-lagged maximum coherence is qualitatively consistent with *Austin and Barth's* [2002] estimate of an 8 day relaxation timescale in their empirical, local, linear model of the wind-driven upwelling response.

[30] Alongshore wind stress and near-surface ocean temperature time series from NDBC 46050 for the May–August time period during 1992–2004 were examined to determine if the 20 day ISOs observed during COAST were typical of this region. Complete time series were available for nine of these years, while 1994, 1996, 1997 and 1999 had significant data gaps. Seven of the 9 years (one of which is 2001) exhibited significant oscillations with periods around 20 days in both wind stress and near-surface ocean temperature. As is the case for 2001 (Figure 15), there is high correlation between alongshore wind stress and near-surface ocean temperature around the 20 day period band for each of these years, when the stress is lagged by several days. Even though the nominal 20 day timescale is much longer than the time it takes for the passage of a synoptic system such as a Gulf of Alaska Low and longer than the typical time between northward wind episodes, the upper ocean temperature response in this period band was very strong during COAST, as is apparent in the middle panels of Figure 15.

[31] The alongshore wind stress has two important periodicities: the synoptic period band associated principally with the passage of Gulf of Alaska Lows (every few days), and the 20 day ISOs. The currents respond quickly to the wind stress, so they follow the synoptic wind fluctuations well [Lentz, 1992; Kosro, 2005]. Once the water is upwelled, much of it remains on the surface, even though the upwelling-favorable winds might slow or even reverse after just a few days. When the upwelling winds subside for a while, the temperature field will respond by warming and mixing. This means the main temperature fluctuation will follow the slower fluctuation in the winds: the 20 day ISOs.

[32] Figure 15 (bottom) shows that the 20 day ISOs in wind stress are coherent with a similar period variation in the north-south position of the atmospheric jet stream (JS). For this analysis, the JS position is taken to be the latitude, along 125°W longitude, of the strongest horizontal gradient in the height of the 200 mb surface, determined from 6 hourly NCEP reanalysis pressure maps. The opposite phasing of the two time series (northward JS position correlates with southward winds off Oregon) can be interpreted as follows. The North Pacific High will “build in” as the JS moves to the north, and will thereby bring stronger southward winds off Oregon (see for example Figure 16, below). When the JS is in a northward location, Gulf of

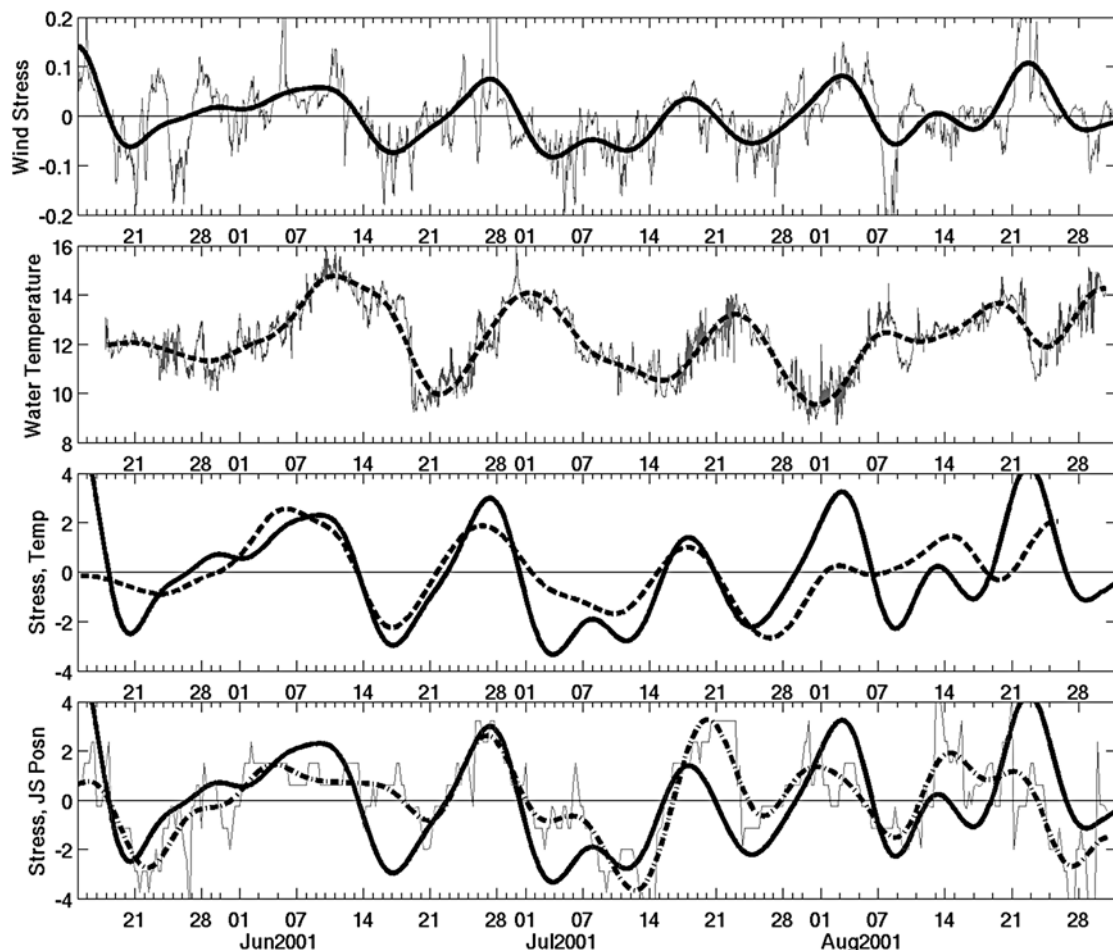


Figure 15. (top) Time series of northward wind stress at the NDBC 46050 buoy (thin line is measured, thick line is 8-DLP), (top middle) upper ocean temperature from SMS (thin line is measured, thick dashed line is 8-DLP), and (bottom middle) these two 8-DLP time series shown together with a 5 day lead applied to the SMS temperature and the stress scaled to fit the vertical axis. Note the sequence of intraseasonal temperature oscillations with periods near 20 days and the high visual coherence these have with the stress oscillations. The correlation coefficient between these two 8-DLP time series is 0.61, which is significant at the 95% level. (bottom) Wind stress time series together with the time series of jet stream position along 125°W (thin is measured, thick dot-dash line is 8-DLP; vertical axis is degrees of latitude for jet stream position, same scale for stress as used in panel above). The jet stream position curves have been inverted so that a southward position is toward the top of the panel. Note the strong visual coherence between the stress and jet position time series. The correlation coefficient between these two 8-DLP time series is 0.55, which is significant at the 95% level.

Alaska Lows may still be present, but their typical eastward tracks are farther from the COAST region and so do not affect the wind stress there. When the JS moves to the south, it brings with it the traveling Gulf of Alaska Lows (see for example, Figure 20, below), which can pass through the COAST region and temporarily change the Oregon winds to northward, thereby decreasing (and sometimes reversing) the low-pass-filtered southward wind stress. This strongly suggests the roughly 20 day positional variations in the JS are the cause of the 20 day wind stress oscillations observed at NDBC 46050. This is consistent with the recent findings of *Lott et al.* [2001] and *Ghil et al.* [2003], who suggest that the JSs interaction with large-scale topography can drive ISOs in large-scale atmospheric circulation patterns. They provide observational evidence that such mountain-

induced torques play a key role in 15–30 day oscillations of the Northern Hemisphere’s dominant circulation patterns.

5. Marine Atmospheric Boundary Layer (MABL)

5.1. MABL During Southward Winds

[33] Southward, upwelling-favorable winds prevailed in the COAST region for about 75% of the study period (Figure 4). Individual southward wind episodes lasted from a few days to about 2 weeks, and during these the North Pacific High dominated the surface pressure field. The aircraft measured the MABL during southward winds on 14 flights, and here we present views of several atmospheric variables measured during flight 15 (24–25 July), as these are exemplary of the MABL during southward winds.

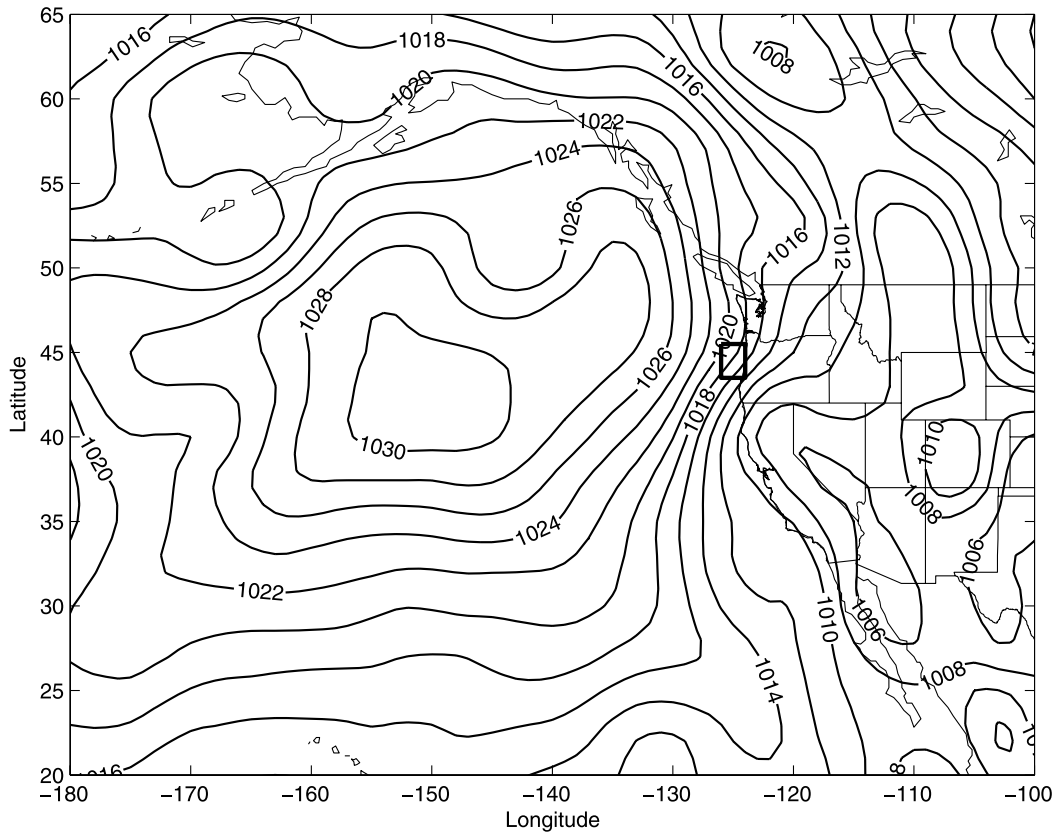


Figure 16. Surface atmospheric pressure field (mb) for 0000 UTC on 25 July, at about the midpoint of flight 15. The North Pacific High covered the entire COAST region at the time and was causing southward winds there, the typical pattern for episodes of southward winds off Oregon. Also note that there was no Gulf of Alaska Low present at this time in the region, and the Thermal Low extended reasonably far north, helping strengthen the southward winds along Oregon and northern California.

Figure 4 shows that southward winds of about $5\text{--}8\text{ m s}^{-1}$ began roughly 6 days prior to this flight and they continued throughout the flight and for 3 more days before being interrupted by a northward wind event. Diurnal variations in the wind strength were relatively small at both NDBC 46050 and MB from 23 through 26 July. The surface atmospheric pressure map for the midpoint of flight 15 is shown in Figure 16, and the dominance of the North Pacific High is apparent.

[34] In Figure 17 (top), a three-dimensional perspective of the atmosphere and ocean throughout the COAST area during flight 15 is shown. As is typical for southward winds off central Oregon, there was a well established temperature

inversion layer, which separated cool, moist air in the MABL below from warm, dry air above. The inversion layer was about 250 m thick and had a strength (vertical temperature difference across the inversion) of about $8^{\circ}\text{--}9^{\circ}\text{K}$ in potential temperature (about 6°K in situ temperature). The inversion base was positioned at about 500 m altitude, but it sloped downward slightly toward shore by about 1 m km^{-1} . For comparison, *Neiburger et al.* [1961] found a typical inversion slope to be 2 m km^{-1} off the northern California coast.

[35] The lateral density gradient due to the 24–25 July inversion slope implies a thermal wind shear of about 10^{-2} s^{-1} . The sense of this shear is to increase southward wind

Figure 17. Three-dimensional views of the atmospheric potential temperature and oceanic in situ temperature fields ($^{\circ}\text{C}$) and near-surface winds (m s^{-1}) for 2 different days in the COAST study region. (top) Period of 24–25 July, which was a day typical of southward winds and fully developed oceanic upwelling. The base of the atmospheric temperature inversion can be seen at about 500 m, and there was a general downward slope of the inversion toward shore, which gave somewhat higher southward wind speeds below the inversion base. The region of cooler air temperature and slower southward wind speed below about 200 m and within about 50 km of the coast is the stable internal boundary layer that had formed above the cool, upwelled surface waters there. The separated upwelling jet in the ocean [*Barth et al.*, 2005] can be seen in the oceanic surface temperature pattern. (bottom) A similar presentation from a northward wind case, 1–2 August. There was little atmospheric stratification, and the wind speeds were slower and less sheared vertically than in the southward wind case. Note also the cooler air temperatures above about 500 m, as compared to the top figure. Some remnant cool, upwelled water can be seen at the ocean surface near the coast. Comparisons of individual profiles from these 2 days are given below in Figure 21. (Note that the wind vectors were measured on a slant profile during either a climb or a descent by the aircraft.)

speed as one moves downward through the inversion layer. Note in Figure 17 (see also Figure 21 below) that the southward wind speed is generally greatest below the inversion layer. The observed southward wind speed

difference across the 250-m-thick inversion layer for this section was around 3 m s^{-1} , quite close to the implied thermal wind shear. Wind shears through the inversion layer similar to this were observed on about half of the aircraft

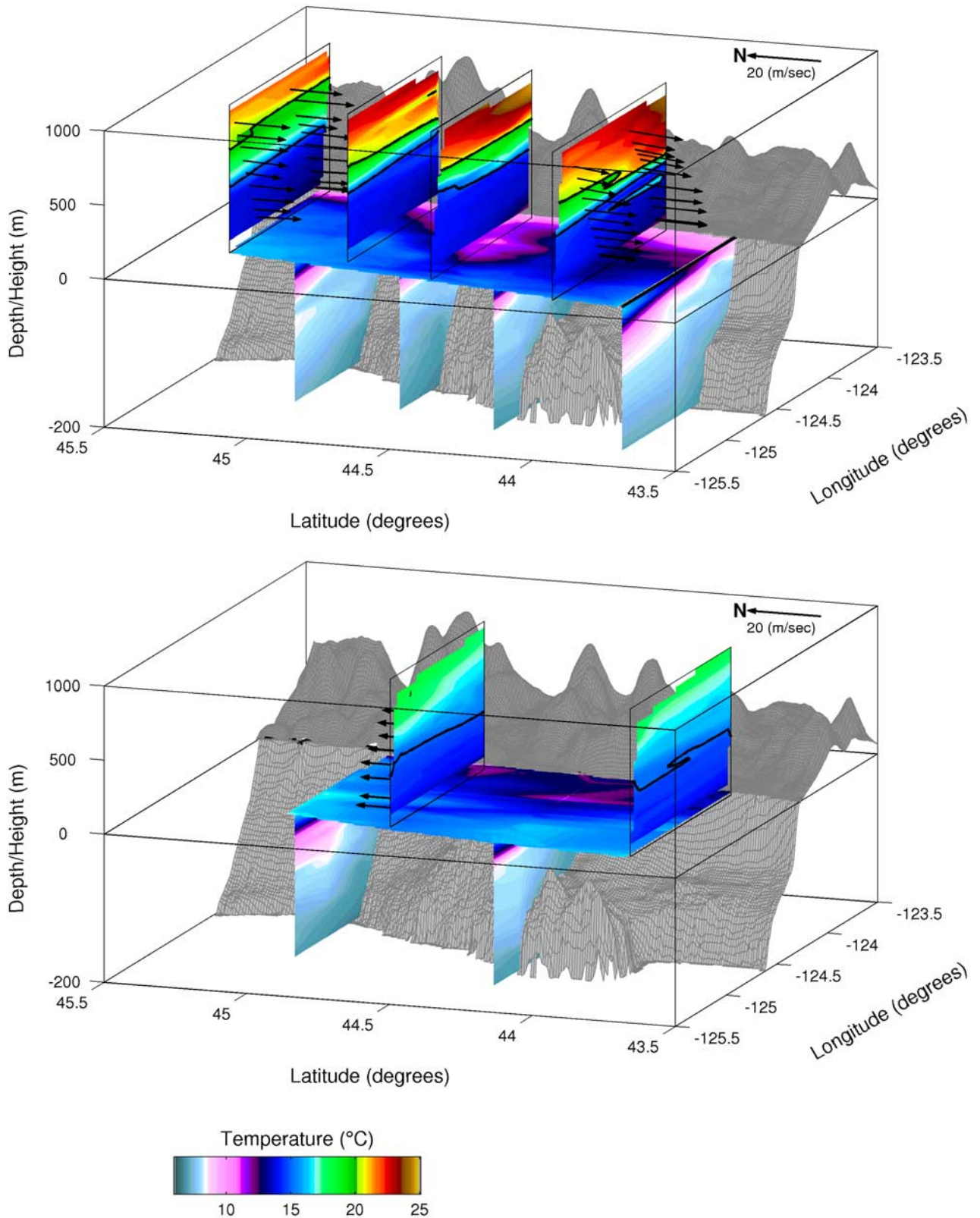


Figure 17

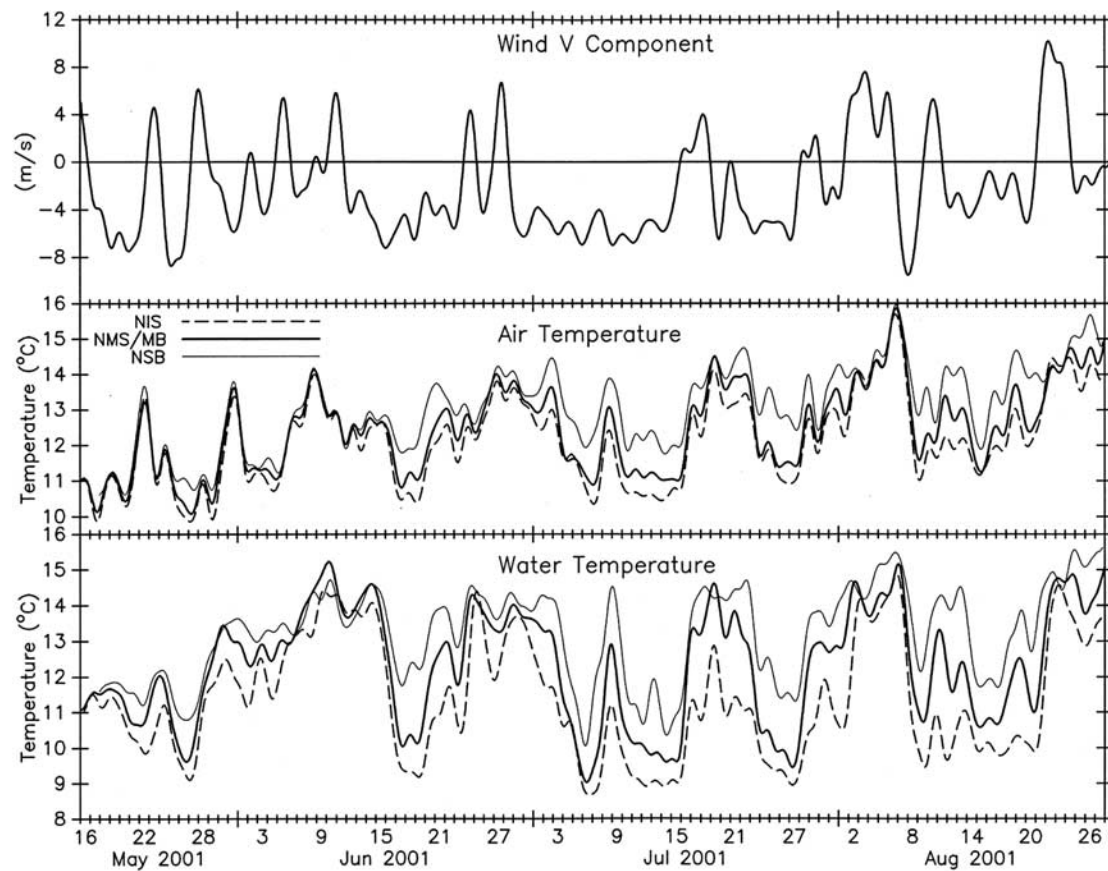


Figure 18. Forty hour low-pass-filtered SAT and near-surface ocean temperature at NIS (dashed), NMS/MB (bold), and NSB (thin) along with northward wind speed measured at MB.

profiles flown during southward winds, and these were mostly over the shoreward half of the flight area; that is, within about 30–40 km of the coastline (see Figure 1). Other profiles during southward winds had relatively constant wind strength through the inversion. When present, such wind shear is an important aspect of the MABL structure in terms of oceanic forcing, as without the increase in the southward wind strength below the inversion the wind stress on the ocean surface would be less. Low-level, southward wind jets have been observed in coastal regions to the south of the COAST study area [Beardsley *et al.*, 1987; Edwards *et al.*, 2001], and they have been similarly related to inversion slope. These earlier observations show, however, that the wind jets off northern California are typically stronger than off central Oregon, probably because of stronger orographic effects on the MABL winds and greater stratification there.

[36] In examining data from all COAST aircraft flights, Meaux [2004] found that there was a temperature inversion similar to that shown in Figure 17 within the lowest 1,000 m of the atmosphere for 10 of the 14 flights for which the daily average wind at NDBC 46050 was greater than 3 m s^{-1} toward the south. For these 10 flights, the MABL inversion had the following mean properties (std. error of estimate of each mean is in parentheses): base height = 458 (51) m, strength (potential temperature) = 7.0 (0.7) $^{\circ}\text{K}$, thickness = 250 (23) m, cross-shore slope = 2.3 (0.3) m km^{-1} , wind shear = 1.3×10^{-2} (0.3×10^{-2}) s^{-1} .

These values suggest that the 24–25 July structure shown in Figure 17 is typical of conditions for central Oregon during summertime southward winds when the inversion is found below 1000 m. For 3 more of the 14 southward wind flights, the inversion layer was found above 1000 m, which is above the height of most mountain peaks in the Coast Range within the study area. As a result, marine air below the inversion was not well confined to the coastal area, and some marine air extended over the mountain tops into inland areas. For the remaining southward wind flight, the aircraft flew high enough to observe just the inversion base, which was near 1500 m. Elliott and O'Brien [1977], using data from aircraft flights during the 1973 CUE-II program, found a similar range of inversion heights during southward winds, noting additionally that there were occasions when no temperature inversion was found below 1500 m.

5.2. Upwelling Effect on Boundary Layer Temperature

[37] Samelson *et al.* [2002] presented indirect evidence, derived from a combination of in situ observations in 1999 and mesoscale meteorological models, for an upwelling effect on SAT of 1° – 5°C over 12–24 hours. To examine this further, five of the COAST moorings were instrumented with SAT sensors (see section 2.1). With the onset of southward, upwelling-favorable winds the near-surface ocean temperature typically decreased, with a greater decrease closer to the coast (Figure 18). A similar

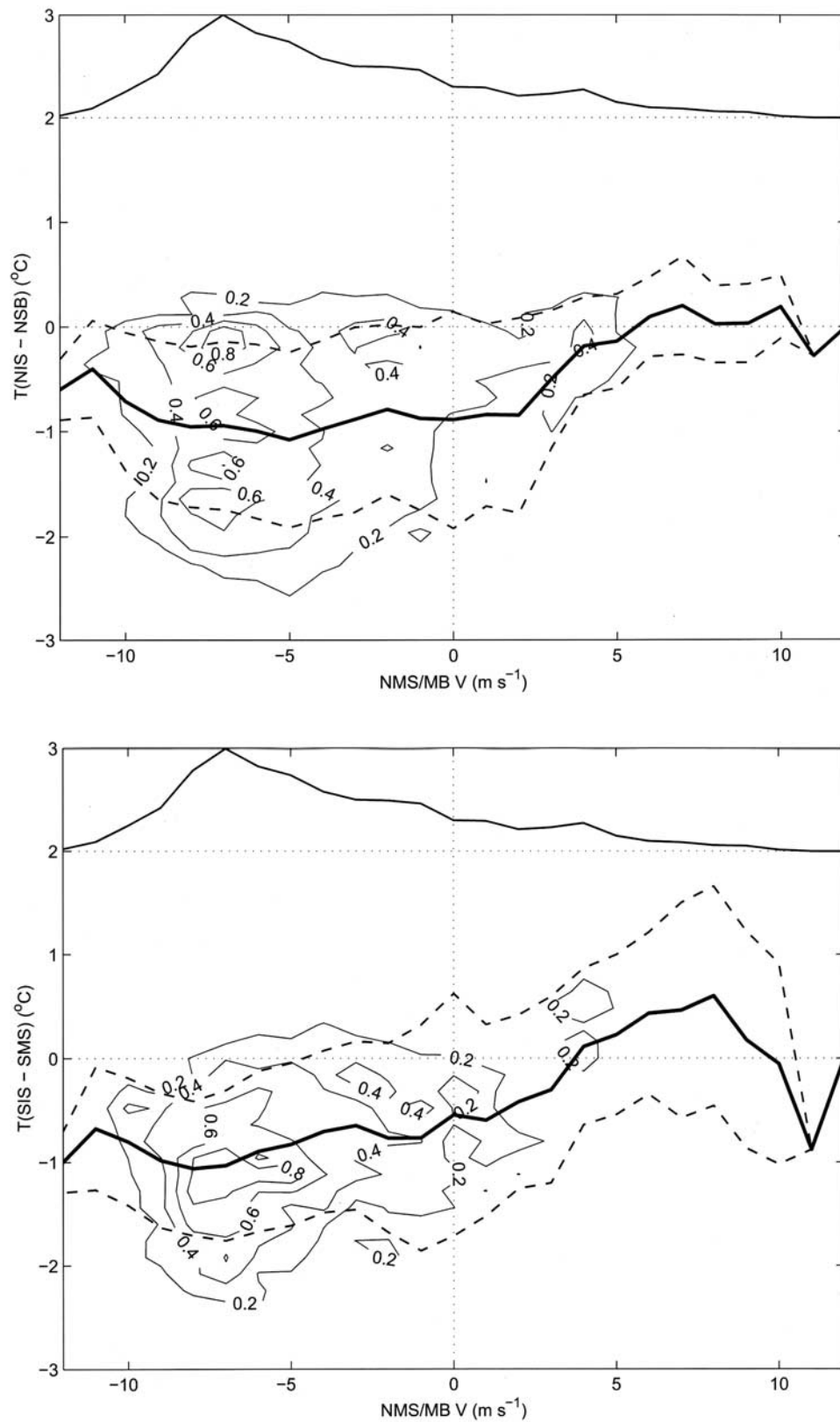


Figure 19. Histogram of (top) northern and (bottom) southern inshore-offshore SAT differences versus SAT difference and alongshore wind at the COAST meteorological buoy. Histograms are normalized by their maximum values. The mean (thick solid line) and standard deviation (dashed line) SAT differences versus alongshore wind are also shown. For reference, the histogram of the alongshore wind distribution (thin solid line), normalized by its maximum value and offset by 2, is shown in the top part of each panel.

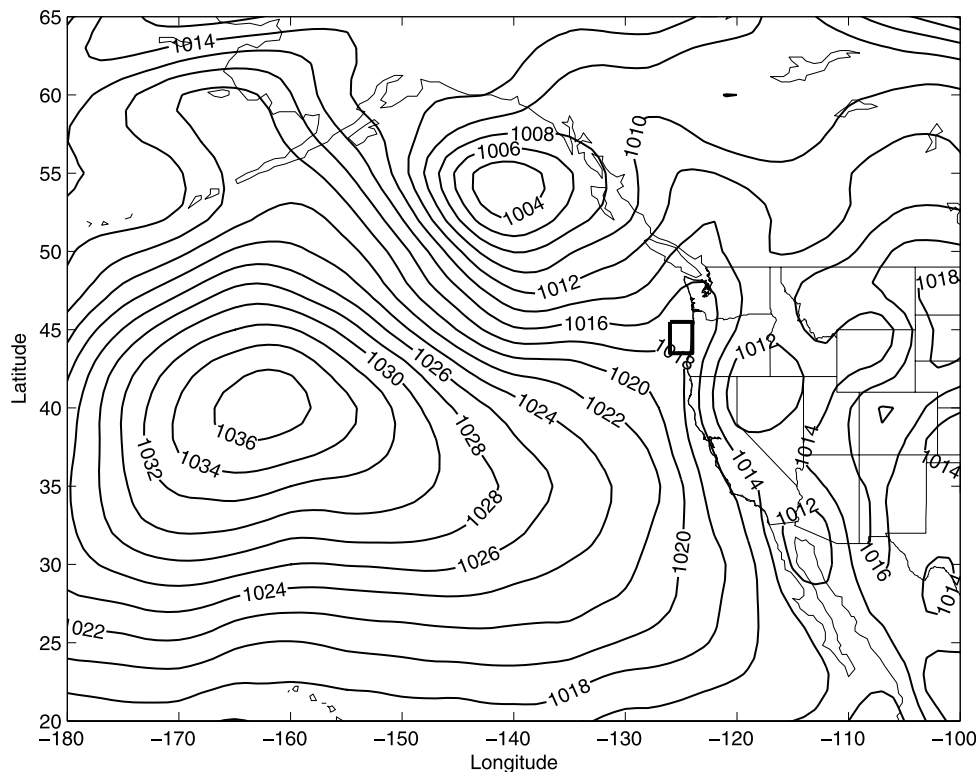


Figure 20. Surface atmospheric pressure field for 0000 UTC on 2 August, at about the midpoint of flight 22. A Gulf of Alaska Low was centered about 55°N, 140°W, and its southern extent was causing northward winds in the COAST area at this time. This low continued its eastward progression and kept the winds northward at COAST for another 3 days. This is typical for episodes of northward winds off Oregon that are the result of a Gulf of Alaska Low.

low-frequency response is seen in the corresponding SAT, with inshore values typically 1°C lower than those offshore during upwelling conditions. These results are further demonstrated for both the North Array and the South Array, with histograms of inshore-offshore SAT differences versus alongshore wind (Figure 19). For southward winds, mean inshore-offshore SAT differences were similar in the south and the north. For northward winds, there was a tendency for reversal of the SAT difference in the south, with slightly cooler temperatures offshore. Deviations about the mean were also somewhat larger in the south for northward winds. Extreme temperature differences (not shown) were generally larger in the south than the north, possibly due to large offshore near-surface ocean temperature anomalies in the complex oceanic flow field over and around Heceta Bank [Barth *et al.*, 2005; Kosro, 2005].

[38] These mooring observations are consistent with the aircraft observations, which show the development of a cool internal boundary layer (IBL) adjacent to the coast during upwelling. Within the MABL between the inversion base and the sea surface, the potential temperature was quite uniform, except immediately above the ocean surface and within about 50 km of shore during southward winds (Figure 17; see also Figure 21, below). There the air was directly over the cool water that had recently upwelled due to the upwelling-favorable wind stress. This cooler air had been flowing over the upwelled water mass for tens to

perhaps a few hundred km before being measured by the aircraft, and it had cooled as a result of enhanced sensible heat flux into the colder surface waters. Buoy data during this time show the sensible heat flux was about 10 W m⁻² into the ocean (Figures 5a and 5b), and it produced the cool IBL, similar to that generated when warm air flows from land to a cooler ocean surface [Hsu, 1983; Garratt, 1990; Rogers *et al.*, 1995]. When present, the IBL grows in thickness in the downwind direction, beginning where the air crosses the upwelling SST front and first encounters the cool, upwelled water. Close to shore on the southernmost COAST aircraft section (line 7 in Figure 1), the IBL was typically observed to have a thickness of about 200 m. The IBL thickness was determined by examining individual profiles of air temperature, humidity, and wind speed (see Figure 21 below).

[39] In addition to lower air temperatures, lower wind speeds were often observed within the IBL as well. There are two reasons for this: first, the lateral density gradient caused by the cooler IBL air close to the coast gives a thermal wind shear that will tend to slow the air closer to the ocean surface, and second, the increased stability within the IBL reduces the depth of the stress boundary layer, thereby increasing the vertical divergence of the turbulent stress that is decelerating the near-surface flow. The lower wind speeds over the cool, upwelled waters close to the coast resulted in a positive wind stress curl on the ocean surface, likely driving upward Ekman

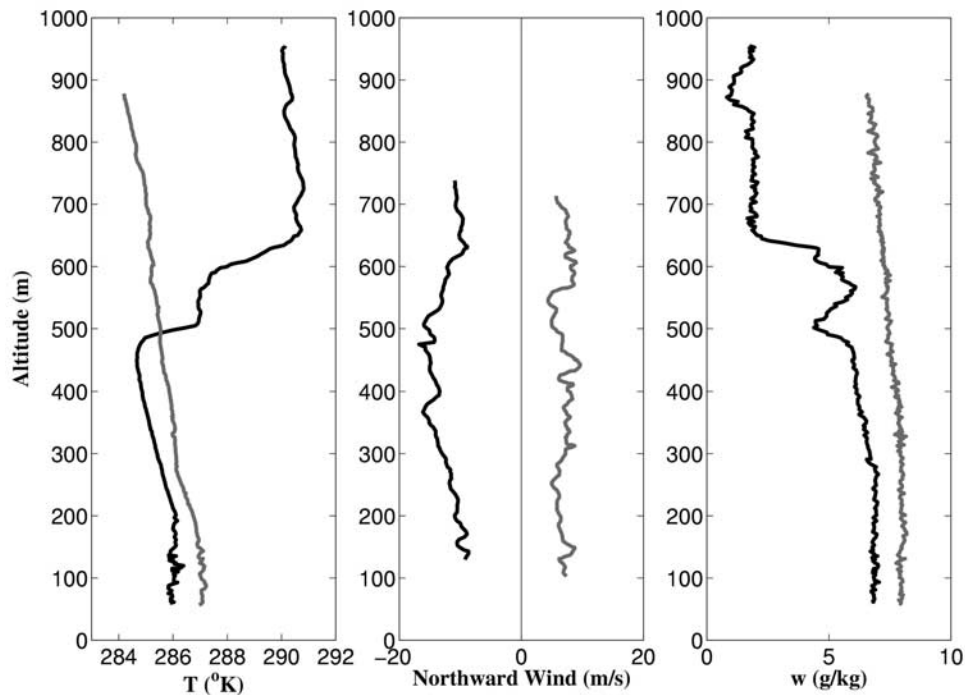


Figure 21. Profiles of in situ temperature, northward wind speed, and mixing ratio measured over the inner portion of the central COAST study region for southward winds (black curves, 24–25 July) and northward winds (shaded curves, 1–2 August). This comparison shows the presence (absence) of a temperature inversion during southward (northward) wind conditions. The presence of the moderate wind jet below the inversion for southward winds (black curve, middle panel) is also apparent, while there was no wind jet during northward winds (shaded curve, middle panel). The mixing ratio profile for southward winds shows the transition within the inversion from moist air in the mixed layer (between the sea surface and the base of the inversion) to dry air above the inversion. The mixing ratio profile during northward winds shows moist air to extend to at least 900 m. The 24–25 July temperature profile below 200 m was within the internal boundary layer (IBL), with cool temperatures and a lesser lapse rate observed there.

pumping. Using wind stresses computed from MB and NDBC 46050 data, an Ekman pumping rate of about 1 m d^{-1} was estimated for times when southward winds prevailed, and thus when the cool IBL was presumed to be present. This is a small rate compared to that due to the Ekman transport divergence imposed by the presence of the coastline. Since the IBL-induced curl reduces the stress at the coast, it represents a spreading of the upwelling over a greater offshore extent than would be the case with no IBL, rather than an intensification of the total local upwelling.

5.3. MABL During Northward Winds

[40] Fifteen episodes of northward winds occurred during the study period, accounting for about 25% of the time (Figure 4). As noted above, the typical cause of a northward wind episode was the passage of a Gulf of Alaska Low, usually progressing eastward along a trajectory that took the storm center to the north of the COAST region but allowed the southern portion of the cyclonic wind system to impact central Oregon. This was the case for flight 16, which took place on 1–2 August. The surface pressure field from about the midpoint of the flight shows a Gulf of Alaska Low passing to the north of the study area closely enough to bring several days of northward winds to COAST (Figure 20).

[41] The MABL structure observed during flight 16 was quite uniform throughout the study area, with no temperature inversion and little wind shear below 900 m (Figure 17, bottom). This is in contrast to the conditions described above for southward winds: a well established temperature inversion and wind jet below the inversion. These differences can also be seen in Figure 21, which shows profiles of in situ temperature, northward wind velocity and mixing ratio measured at a location in the central COAST study area on both 1–2 August (northward winds) and 24–25 July (southward winds). This comparison shows the presence (absence) of the in situ temperature inversion during southward (northward) wind conditions. Also, the signature of the cool IBL can be seen for the southward wind case in the temperature profile from 24–25 July. The nearly constant in situ temperature below 200 m shows the existence of the IBL at this time, and the change in the temperature lapse rate at 200 m identifies that as the top of the IBL. The wind speed profile does not extend into the IBL far enough to show the typical speed decrease there. The presence of the wind jet below the inversion for southward conditions is also apparent, while in contrast there was no wind jet during northward winds, which was the typical observation. The mixing ratio profile for southward winds shows dry air above the inversion; the

comparable profile for northward winds shows humid air to have extended at least to 900 m.

6. Summary

[42] During the summer 2001 COAST field experiment along the central Oregon coast, in situ and remote observations and operational model estimates of low-level atmospheric variables and air-sea fluxes were obtained. From May through August 2001, southward wind stresses of order $0.05\text{--}0.1\text{ N m}^{-2}$ occurred about 75% of the time. The longest period of southward stress was from mid-June through the end of July, with only two brief reversals to northward stress. Fluctuations in coastal winds along the Washington and central Oregon coast were correlated with variability in the Aleutian Low pressure center, and along northern California and Oregon with variability in the North Pacific High pressure center, while correlations with the continental Thermal Low were small. Mean wind stress and mean total heat flux into the ocean increased southward along the Oregon coast and were maximum in the region between Cape Blanco and Point Arena. Sensible-plus-latent heat fluxes were mostly from the ocean into the atmosphere until early July, and weakly from the atmosphere into the ocean in July and August. Fluctuations in both of these fluxes on timescales typical of synoptic weather variations were observed throughout the study period. A semidiurnal peak in surface air temperature at several COAST moorings was observed, and it was apparently forced indirectly by nonlinear internal ocean tides. The diurnal cycle of wind stress was similar in both southward and northward wind conditions. When the mean wind stress is included, however, the sum of mean plus diurnal stress results in the following pattern: the greatest (least) alongshore wind stress near sunset for southward (northward) winds, and the least (greatest) alongshore stress in the morning hours for southward (northward) winds. Several intraseasonal oscillations in upper ocean temperature, which had peak-to-peak amplitudes of about 4°C and periods of around 20 days, were correlated with alongshore wind stress fluctuations on that same timescale. The stress fluctuations were, in turn, correlated with intraseasonal oscillations in the north-south position of the jet stream. When the jet stream was positioned to the north, the winds in the COAST study area were strongly toward the south. When the jet stream was to the south it brought Gulf of Alaska Lows past the COAST region, which reversed the winds to the north for 1 to several days. The MABL was observed to have a strong temperature inversion during southward winds, while there was little to no temperature stratification observed during northward winds. For southward winds, a moderate downward slope in the inversion toward shore was typical and it gave rise to a thermal wind shear that produced a mild southward wind jet near the base of the inversion. Also, a stable IBL formed within the marine atmospheric boundary layer over the cool upwelled water adjacent to the coast, with surface air temperature typically 1°C lower there as compared to farther offshore. Slightly slower surface wind speeds were typical within the IBL, and this produced a wind stress curl sufficient to drive and upward Ekman pumping of

about 1 m d^{-1} . This tended to spread the upwelling over a wider area than would have been the case without the IBL.

[43] **Acknowledgments.** This research was supported by the National Science Foundation Coastal Ocean Processes program under grants OCE-9907854 and OCE-9907919. We are grateful to D. Chelton, M. Schlax, and M. Freilich for providing the QuikSCAT wind stress data. We thank J. Miller and M. Sessions for their help in instrumenting and flying the aircraft during COAST. We appreciate the efforts of W. Waldorf and D. Root for building and deploying the moorings and S. Gard for data archiving and analysis. Comments from anonymous reviewers were helpful in improving the presentation.

References

- Austin, J. A., and J. A. Barth (2002), Variation in the position of the upwelling front on the Oregon shelf, *J. Geophys. Res.*, *107*(C11), 3180, doi:10.1029/2001JC000858.
- Bane, J. M., S. M. Haines, L. Armi, and M. H. Sessions (1995), The California coastal marine layer: Winds and thermodynamics, *Tech. Rep. CMS-95-1*, Aircraft Measure. Prog. Univ. of N. C., Chapel Hill.
- Barth, J. A., S. D. Pierce, and R. M. Castelao (2005), Time-dependent, wind-driven flow over a shallow midshelf submarine bank, *J. Geophys. Res.*, *110*, C10505, doi:10.1029/2004JC002761.
- Beardsley, R., C. Dorman, C. Friehe, L. Rosenfeld, and C. Winant (1987), Local atmospheric forcing during the Coastal Ocean Dynamics Experiments 1 and 2: 1. A description of the marine boundary layer and atmospheric conditions over a northern California upwelling region, *J. Geophys. Res.*, *92*, 1467–1488.
- Beardsley, R. C., E. P. Dever, S. J. Lentz, and J. P. Dean (1998), Surface heat flux variability over the northern California shelf, *J. Geophys. Res.*, *103*, 21,553–21,586.
- Bielli, S., P. Barbour, R. Samelson, E. Skillingstad, and J. Wilczak (2002), Numerical simulations of the diurnal cycle along the Oregon coast during summertime northerly flow, *Mon. Weather Rev.*, *130*, 992–1008.
- Black, T. L. (1994), The new NMC mesoscale Eta Model: Description and forecast examples, *Weather Forecasting*, *9*, 265–278.
- Boyd, T., M. D. Levine, P. M. Kosro, S. R. Gard, and W. Waldorf (2002), Observations from moorings on the Oregon continental shelf, May–August 2001, *Data Rep. 190, COAS Ref. 2002-6*, Oreg. State Univ., Corvallis.
- Coastal Ocean Processes (1998), Coastal Ocean Processes (CoOP): Wind-driven transport science plan, *Tech. Rep. UMCES TS-170-98*, Cent. for Environ. Sci. Univ. of Md., Cambridge.
- Edwards, K. A., A. Rogerson, C. Winant, and D. Rogers (2001), Adjustment of the marine atmospheric boundary layer to a coastal cape, *J. Atmos. Sci.*, *58*, 1511–1528.
- Elliott, D. L., and J. J. O'Brien (1977), Observational studies of the marine boundary layer over an upwelling region, *Mon. Weather Rev.*, *105*, 86–105.
- Fairall, C. W., E. F. Bradley, D. P. Rogers, J. B. Edson, and G. S. Young (1996), Bulk parameterization of air-sea fluxes for tropical ocean-global atmospheric coupled-ocean atmosphere response experiment, *J. Geophys. Res.*, *101*, 3747–3764.
- Garratt, J. R. (1990), The internal boundary layer—A review, *Boundary Layer Meteorol.*, *50*, 171–203.
- Ghil, M., D. Kondrashov, F. Lott, and A. W. Robertson (2003), Intraseasonal oscillations in the mid-latitudes: Observations, theory, and GCM results, paper presented at the Workshop on Simulation and Prediction of Intra-Seasonal Variability, ECMWF/CLIVAR, Reading, U. K., 3–6 Nov.
- Halliwel, G., Jr., and J. S. Allen (1987), The large-scale coastal wind field along the west coast of North America, 1981–1982, *J. Geophys. Res.*, *92*, 1861–1884.
- Hsu, S. A. (1983), On the growth of a thermally modified boundary layer by advection of warm air over a cooler sea, *J. Geophys. Res.*, *88*, 771–774.
- Johnson, A., and J. J. O'Brien (1973), A study of an Oregon sea breeze event, *J. Appl. Meteorol.*, *12*, 1267–1283.
- Kalnay, E., et al. (1996), The NCEP/NCAR 40-Year Reanalysis Project, *Bull. Am. Meteorol. Soc.*, *77*, 437–471.
- Koopmans, L. H. (1974), *The Spectral Analysis of Time Series*, Elsevier, New York.
- Kosro, P. M. (2005), On the spatial structure of coastal circulation off Newport, Oregon, during spring and summer 2001 in a region of varying shelf width, *J. Geophys. Res.*, doi:10.1029/2004JC002769, in press.

- Large, W. G., and S. Pond (1981), Open ocean momentum flux measurements in moderate to strong winds, *J. Phys. Oceanogr.*, *11*, 324–336.
- Lentz, S. J. (1992), The surface boundary layer in coastal upwelling regions, *J. Phys. Oceanogr.*, *22*, 1517–1539.
- Liu, W. T. (2002), Progress in scatterometer application, *J. Oceanogr.*, *58*, 121–136.
- Lott, F., A. W. Robertson, and M. Ghil (2001), Mountain torques and atmospheric oscillations, *Geophys. Res. Lett.*, *28*, 1207–1210.
- Meaux, M. F. (2004), The marine atmospheric boundary layer over the Oregon coastal upwelling system during summer 2001, M. S. thesis, Mar. Sci. Dep., Univ. of N. C., Chapel Hill.
- Naderi, F. M., M. H. Freilich, and D. G. Long (1991), Spaceborne radar measurement of wind velocity over the ocean: An overview of the NSCAT scatterometer system, *Proc. IEEE*, *79*, 850–866.
- Neiburger, M., D. S. Johnson, and C. Chien (1961), Studies of the structure of the atmosphere over the eastern Pacific Ocean in summer, I, The inversion over the eastern North Pacific Ocean, *Univ. Calif. Publ. Meteorol.*, *1*, 1–94.
- Nuss, W. A., et al. (1999), Coastally trapped wind reversals: Progress toward understanding, *Bull. Am. Meteorol. Soc.*, *81*, 719–743.
- Perlin, N., R. M. Samelson, and D. B. Chelton (2004), Scatterometer and model wind and wind stress in the Oregon-California coastal zone, *Mon. Weather Rev.*, *132*, 2110–2129.
- Reznik, G. M., and R. Grimshaw (2002), Nonlinear geostrophic adjustment in the presence of a boundary, *J. Fluid Mech.*, *471*, 257–283.
- Rogers, D. P., D. W. Johnson, and C. A. Friehe (1995), The stable internal boundary layer over a coastal sea. Part I: Airborne measurements of the mean and turbulence structure, *Mon. Weather Rev.*, *52*, 667–683.
- Samelson, R. M., P. Barbour, J. Barth, S. Bielli, T. Boyd, D. Chelton, P. Kosro, M. Levine, E. Skillingstad, and J. Wilczak (2002), Wind stress forcing of the Oregon coastal ocean during the 1999 upwelling season, *J. Geophys. Res.*, *107*(C5), 3034, doi:10.1029/2001JC000900.
- Smith, R. L., and K. H. Brink (1994), Coastal ocean processes: Wind-driven processes on the U. S. west coast, *Tech. Rep. WHOI-94-20*, Woods Hole Oceanogr. Inst., Woods Hole, Mass.
- Thiébaux, J., E. Rogers, W. Wang, and B. Katz (2003), A new high-resolution blended real-time global sea surface temperature analysis, *Bull. Am. Meteorol. Soc.*, *84*, 645–656.
- Winant, C. D., C. E. Dorman, C. A. Friehe, and R. C. Beardsley (1988), The marine layer off northern California: An example of supercritical channel flow, *J. Atmos. Sci.*, *45*, 3588–3605.

J. M. Bane and S. M. Haines, Department of Marine Sciences, University of North Carolina, 12-7 Venable Hall, Chapel Hill, NC 27599-3300, USA. (bane@unc.edu)

T. Boyd, P. M. Kosro, M. D. Levine, N. Perlin, and R. M. Samelson, College of Oceanic and Atmospheric Sciences, Oregon State University, 104 COAS Admin Building, Corvallis, OR 97331–5503, USA.

M. F. Meaux, Global Change Data Center, NASA/Goddard Space Flight Center, Building 32, Room S130D, Greenbelt, MD 20771, USA.